



Effects of bora wind on physical and biogeochemical properties of stratified waters in the northern Adriatic

A. Boldrin,¹ S. Carniel,¹ M. Giani,² M. Marini,³ F. Bernardi Aubry,¹ A. Campanelli,³ F. Grilli,³ and A. Russo⁴

Received 31 March 2008; revised 30 March 2009; accepted 26 May 2009; published 25 August 2009.

[1] Wind forcing plays a key role in controlling the water column structure and circulation in the northern Adriatic Sea. Through shipboard observations and numerical modeling, we have documented the changing of oceanographic features before, during, and after a sequence of cold northeasterly bora wind pulses that occurred during stratified conditions in late September 2002. High-resolution meteorological, hydrodynamic, and wave model outputs were related to in situ observations of hydrologic parameters, dissolved nutrients and oxygen, suspended matter biogeochemical properties, and phytoplankton. The bora intensified the southward flowing coastal current along the Italian coast, establishing a frontal system that typically exists in winter. The bora also caused complete vertical mixing to 20–25 m in the water column, an influx of warm salty water from the south along the Croatian coast, and increased resuspension and southward transport of bottom sediments for the combined effects of currents and waves. The effects on the bottom were limited to the western coastal belt, as in the deeper central part of the basin hypoxic conditions were present during the whole observing period. During the bora, the concentration of inorganic dissolved nutrients in the bottom water increased consistently with the release of nutrients from the sediments and with the mineralization processes. Resuspension of bottom layer sediment represents an important source of nutrients for the water column in this period. The higher level of nutrients was observed together with an increase in phytoplankton biomass, suggesting a potential trigger for the autumnal phytoplankton bloom in the northern Adriatic. Finally, bora events seem to be able to generate a relevant increase of nutrient export from the northern Adriatic through the intensified Adriatic western coastal current, so they could play a relevant role in the nutrient balance of the basin.

Citation: Boldrin, A., S. Carniel, M. Giani, M. Marini, F. Bernardi Aubry, A. Campanelli, F. Grilli, and A. Russo (2009), Effects of bora wind on physical and biogeochemical properties of stratified waters in the northern Adriatic, *J. Geophys. Res.*, *114*, C08S92, doi:10.1029/2008JC004837.

1. Introduction

[2] The frequency and strength of winds strongly influence the water column structure and circulation in the northern Adriatic basin (NA), the northernmost area of the Mediterranean Sea. In particular, the cold northeasterly “bora” wind, occurring frequently in the fall and winter seasons, plays a large role in determining the cooling and mixing of the water column, the circulation patterns and the dense water formation [Hopkins *et al.*, 1999; Poulain and Raicich, 2001].

[3] The bora has a jet-like structure that is characterized by strong horizontal shear due to orographic control (this

katabatic wind is generated by cold and dry air spilling down from passes through the Dinaric Alps). The bora wind pattern typically induces a counterclockwise gyre in the northernmost part of the NA basin, enhancing the Western Adriatic Coastal Current (WACC) [Kuzmić and Orlić, 1987; Orlić *et al.*, 1994; Artegiani *et al.*, 1997; Bergamasco *et al.*, 1999; Zavatarelli *et al.*, 2002].

[4] In addition to strengthening the WACC, the bora can also advect water from the Po delta region offshore, forming a northeastward moving tongue of cold fresh water [Beg Paklar *et al.*, 2001]. Numerical model simulations can provide information about the high spatial and temporal variability that characterizes strong wind events and their effects on the oceanic side.

[5] In regions like the NA, surrounded by complex orography, model resolution must be sufficiently high to resolve the spatial structures in the wind field and the circulation patterns they impose. Early oceanographic models had to scale up wind speeds from under-resolved meteorological models in order to obtain reasonable results [Cavaleri and

¹Istituto di Scienze Marine, CNR, Venice, Italy.

²Department of Biological Oceanography, Istituto Nazionale di Oceanografia e di Geofisica Sperimentale, Trieste, Italy.

³Istituto di Scienze Marine, CNR, Ancona, Italy.

⁴DISMAR, Università Politecnica delle Marche, Ancona, Italy.

Bertotti, 1997; Cavaleri, 2002]. Despite these resolution issues, early numerical studies of the basin circulation were able to suggest the offshore spreading of the Po diluted waters under stratified and bora wind conditions [Malanotte Rizzoli and Bergamasco, 1983; Kuzmić and Orlić, 1987; Zore Armanda and Gačić, 1987; Kuzmić, 1991; Orlić et al., 1994], while the confinement along the western coast of the plume was associated with unstratified and weak wind conditions [Kourafalou, 1999].

[6] Dorman et al. [2006], using in situ observations and model results from the same meteorological model employed in this study, analyzed a strong winter bora episode during February 2003. Book et al. [2007], using current meter observations from 2002 to 2003, determined that the circulation in the NA was strongly affected by wind storm events, with increased southward transport in the WACC. In summer condition, the increase of dynamic in the basin was attributed to the interaction between bora wind and the river discharges [Beg Paklar et al., 2008].

[7] In the last decade, increased computing power and operational meteorology technology has resulted in a proliferation of “limited area” meteorological models which are typically driven by global models at their open boundaries. Their grid spacing is typically 5–10 km, allowing a more accurate description of the orography and better representation of small-scale physics, essential in a high-variability basin such as NA. Limited Area Model Italy (LAMI; Italian implementation of the nonhydrostatic model LM [Steppeler et al., 2003], recently renamed COSMO-I7) meteorological output fields have been employed to force the circulation transport model Regional Ocean Modeling System (ROMS) in several studies obtaining results that agreed well with the extensive data collected in 2002–2003 [Sherwood et al., 2004; Carniel et al., 2009]. A detailed comparison during bora events indicated that this approach captured complex circulation patterns [Lee et al., 2005]. Other successful examples are given by Pullen et al. [2003, 2007] using the meteorological outputs from Coupled Ocean/Atmosphere Mesoscale Prediction System (COAMPSTM) model.

[8] Ocean models driven by high-resolution wind fields have been used to obtain new levels of understanding of the NA. Bignami et al. [2007] analyzed the LAMI-driven ROMS results and proposed new insight on the variability and offshore export of turbid coastal waters in the Adriatic Sea, finding that turbid water was exported offshore the Po delta under bora wind events and in low Po River discharge condition. Several processes occurring in the water column are conditioned directly or indirectly by the wind stress. The sediment transport in NA appears to be strictly related to wind stress, as shown by the importance of resuspension in the sediments transport southward mainly occurring in relation with strong winds [Nittrouer et al., 2004; Harris et al., 2008]. The bora events contribute to enhance the along-shelf advection at the bottom layer, as evidenced by benthic tripod measurements in the shelf western Adriatic area [Fain et al., 2007]. Moreover, the resuspension appears to be responsible for the higher contribution in the total vertical fluxes of particulate matter in coastal areas (in average 34–43% [Giani et al., 2001]). In a similar way, the resuspension could have relevant impact on dissolved nutrient budget, modifying the concentration in overlying

water for mixing with pore waters and enhancing the remineralization near the bottom [Fanning et al., 1982]. Resuspension seems to enhance the fluxes into or out of the sediments for most nutrients, particularly increasing the nitrate + nitrite and silicate fluxes [Tengberg et al., 2003].

[9] Sediments with nutrients and other waterborne material, due to resuspension processes during bora events, are driven southward along the Italian coast [Lee et al., 2005; Marini et al., 2008]. Moreover, in the bottom layer the nutrients derived from microbial degradation and regeneration, at the end of summer season, could represent one of the major factors influencing the phytoplankton production [Mann, 1982] and in the NA the N and P derived from regeneration processes are estimated in $38,400 \text{ } 10^6 \text{ mol a}^{-1}$ and $1065 \text{ } 10^6 \text{ mol a}^{-1}$, respectively, more than 50% of total input of N and P in the basin [Degobbis and Gilmartin, 1990]. Thus, turbulent energy due to the wind stress, causing mixing processes, affects the redistribution of nutrients, planktonic organisms in the water column and the overall biological productivity [Yin et al., 1995; Eslinger and Iverson, 2001; Lewis et al., 2001].

[10] Phytoplankton has limited motility, thus physical processes are of great importance to determine its distribution. The effects of advection and wind-driven mixing on phytoplankton have been studied both with observations and model simulations [Eslinger and Iverson, 2001], finding the spring bloom occurring as a response to the cessation of convective mixing. In the fall, wind-induced mixing of the water column can induce blooms by bringing nutrients from the deep water to the surface, yet the timing and intensity of the bloom can vary considerably depending by the interplay among solar heating, latent and sensible heat losses and wind mixing [Olesen et al., 1999]. Wind and tide can also determine conditions for phytoplankton blooms associated with nutrient input from rivers, as observed in the surface layer of the Rhine Plume [Joordens et al., 2001].

[11] Despite the large number of studies on the physical oceanographic response to bora in NA, few observations on the biogeochemical response of basin in relation to the wind events are available. Moreover, though the effects of bora wind on the Adriatic circulation are well studied, they are focused on the winter situations while the studies of the effects of bora on a stratified basin in summertime are rare: only one episode during summer season was discussed by Beg Paklar et al. [2008] with regard to the physical oceanography. In the present paper it is addressed for the first time the interplay among the physical forcing and the nutrient availability and transformations, suspended matter dynamic and the phytoplankton response under the changing conditions induced by bora wind blowing on stratified water column at the end of the summer season.

[12] Integrating information from high-resolution numerical models (meteorological, hydrodynamical, wave and sediment transport) and sea truth observations, the oceanographic and meteorological framework conditions in the prebora, during bora, and postbora periods are discussed. Dissolved oxygen and inorganic nutrient dynamics are investigated, in the perspective of an increased mixing due to the wind events that caused partial ventilation, higher resuspension of bottom sediments and larger availability of nutrients in the water column. The suspended matter and chlorophyll response to such wind-induced physical pro-

cesses events are then discussed, focusing on the consequences on the phytoplankton productivity and growth, and associated hypothesis on the eutrophication dynamics that characterize the NA.

2. Methods

2.1. Numerical Models

[13] The COAMPS model was used to drive the circulation model over the Adriatic Sea. It is a 3-D operational finite difference, nonhydrostatic, sigma coordinate model developed by the Naval Research Laboratory [Hodur, 1997; Hodur and Doyle, 1998]. COAMPS was run in a reanalysis mode using three nested grids with the finest 4 km grid mesh centered over the Adriatic Sea. The two outer meshes are a 12 km grid covering the majority of the Mediterranean and a 36 km resolution European grid, where the global NOGAPS (Navy Operational Global Atmospheric Prediction System) model provides lateral boundary conditions. COAMPS assimilated data from radiosondes, surface satellite, and aircraft observations, and in this application we used 3 hourly outputs. Further details and an evaluation of the COAMPS system are documented by Hodur *et al.* [2001] and (for the Adriatic reanalysis) by Pullen *et al.* [2003].

[14] The oceanic circulation was simulated using ROMS version 2.2 (<http://www.myroms.org>). The model solves finite difference approximations of the three-dimensional Reynolds-averaged equations for conservation of mass, momentum, and heat using a generic length scale turbulence approach proposed by Umlauf and Burchard [2003], with the implementation of Warner *et al.* [2005]. Wind-driven circulation, mixing, and heating or cooling of surface waters were calculated using the COARE 3.0 bulk flux algorithms [Fairall *et al.*, 2003] with shortwave radiation, wind, air temperature, humidity, and atmospheric pressure from COAMPS, but with sea surface temperature (SST) from ROMS. Initial water temperatures and salinities were set by interpolating from hydrographic data collected during September 2002 surveys. The model covers the Adriatic area using a curvilinear orthogonal grid with a resolution ~ 4 km in the NA, with 20 vertical levels. Daily averaged time series of fresh water supply from the Po River and from Pescara and Biferno rivers flow in southern Adriatic [Sherwood *et al.*, 2004; Harris *et al.*, 2008] were supplied; besides, in order to better account for the impact on coastal circulation, the flow of other rivers based on monthly mean values using climatological estimates [Raicich, 1994, 1996] were imposed as well, for a total of 48 rivers. At the southern open boundary, Otranto Straits, both tidal elevation and currents for the main tidal components (M2, S2, K1, O1) were specified, the values resulting from a finite element model of the whole Mediterranean [Cushman-Roisin and Naimie, 2002]. The barotropic open boundary conditions are from Flather [1976] for the 2-D momentum and Chapman [1985] for the tidal elevation. For 3-D passive tracers and baroclinic fields the Orlanski [1976] radiation condition is prescribed. A recursive MPDATA advection is chosen for model the tracers dynamics [Shchepetkin and McWilliams, 2005].

[15] COAMPS winds were used to drive the Simulating Waves Nearshore (SWAN) model [Booij *et al.*, 1999; Ris *et*

al., 1999] using the approach of Signell *et al.* [2005]. SWAN was run in a stand-alone configuration and bottom wave parameters were used by ROMS to compute combined wave-current bottom stress for sediment resuspension as well as the increased drag on the circulation [Harris *et al.*, 2008; Warner *et al.*, 2008]. ROMS can handle an unlimited number of user-defined size classes of noncohesive sediments, each class having fixed attributes (e.g., grain diameter, density, settling velocity, critical shear stress for erosion). ROMS calculates bottom stresses under the combined influence of wave, currents, and mobile sediments. These stresses act as agents for sediment resuspension and bed load transport [Soulsby and Damgaard, 2005].

[16] Harris *et al.* [2008] created the initial sediment bed using information from George *et al.* [2007] and Palinkas and Nittrouer [2007]. The values for fluvial sediment of the Po and Apennine river discharge, mostly deducted from model estimates reached a total of 32.3 Mt a^{-1} [Cattaneo *et al.*, 2003]. A no-gradient condition was applied for sediment concentrations at the Otranto Straits.

2.2. Field Activity and Measurements

[17] Field data were collected in the NA during the Consiglio Nazionale delle Ricerche R/V *Dallaporta* “ANOSSIA” cruise (16–19 September 2002) and during the NATO R/V *Alliance* “ADRIA02” cruise (22 September to 7 October 2002). During these cruises, a network of stations in the NA (Figure 1) were sampled 4–5 times to determine hydrologic, hydrochemical and biological parameters. In particular, 108 stations were sampled between 16 and 19 September, 124 stations were sampled between 22 and 26 September, 89 stations were sampled between 27 and 29 September, 98 stations were sampled between 30 September and 2 October, and 134 stations were sampled between 3 and 7 October.

[18] At each station conductivity-temperature-depth (CTD) casts were obtained, utilizing a SeaBird CTD (SBE 911plus) “Real-Time” Pumped Double Conductivity and Temperature system, equipped with sensor for dissolved oxygen (SBE 43). During the ADRIA02 cruise, CTD was equipped with in situ fluorescence (Chelsea Instrument, AquatrackaIII, 430 nm, 685 nm) and turbidity (Seapoint) sensors, whereas in ANOSSIA cruise a Turner SCUFA sensor for in situ fluorescence + turbidity was utilized. Measurements obtained from optical sensors during ADRIA02 cruise were converted in chlorophyll *a* and total suspended matter, utilizing the linear regression with analytical values as described below.

[19] Water samples for determination of dissolved oxygen (DO) and dissolved inorganic nutrients (ammonia (NH_4), nitrite (NO_2), nitrate (NO_3), orthophosphate (PO_4), and orthosilicate ($\text{Si}(\text{OH})_4$)) were collected during both campaigns at 2 to 5 different depths at selected stations according to the thermohaline structure and to the vertical profiles of turbidity and fluorescence. Samples for suspended matter characterization (total suspended matter (TSM), particulate organic carbon (POC), total particulate nitrogen (TPN), total particulate phosphorus (TPP), chlorophyll *a* (Chl *a*) and phytoplankton species composition and biomass) were collected between 27 September and 2 October. The samples for DO were analyzed on board by the standard Winkler method utilizing an automatic titrator Metrohm,

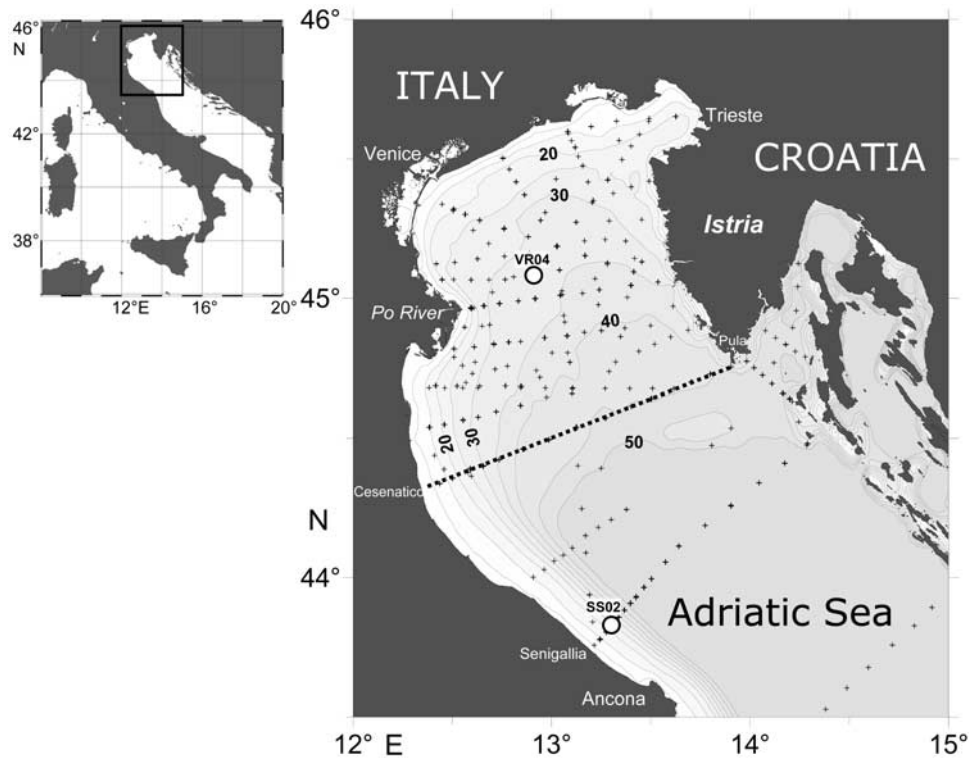


Figure 1. Studied area with isobaths every 5 m. CTD and water sampling stations are reported. Cesenatico-Pula transect is indicated by the dotted line, and stations VR04 and SS02 are indicated by open circles.

with potentiometric measures [Furuya and Harada, 1995]. Winkler DO data were utilized to calibrate the CTD-oxygen sensor (linear regression: $n = 239$, $r = 0.888$, and $P < 0.001$). Nutrient samples were filtered (GF/F Whatman, 25 mm, nominal pore size $0.7 \mu\text{m}$) immediately after the sampling, stored at -20°C in polyethylene vials, and analyzed with a Technicon Autoanalyzer Traacs 800 system. The resulting data were processed with AACE 5.24 software. Total dissolved inorganic nitrogen (DIN) was calculated as $\text{NH}_4 + \text{NO}_2 + \text{NO}_3$.

[20] The samples for analysis of suspended matter were filtered immediately on board using GF/F Whatman filters (25 mm diameter for TSM and POC/TPN, 47 mm diameter for TPP and Chl *a*; $0.7 \mu\text{m}$ nominal porosity) and stored at -20°C . The filters for TSM were preweighted and those for POC/TPN and TPP were precombusted at 450°C for 4 h to eliminate the organic contaminants.

[21] TSM was determined gravimetrically [Strickland and Parsons, 1972]. CTD-turbidity sensor data measured during the ADRIA02 cruise were converted in TSM applying a linear regression ($n = 121$; $r = 0.785$; $P < 0.001$). POC and TPN were determined by Perkin-Elmer 2400-CHN Elemental Analyzer, after removal of inorganic carbon with HCl [Hedges and Stern, 1984]. TPP was determined by HCl 1N extraction after combustion at 550°C for 4 h [Aspila et al., 1976]. The extracts were analyzed by inductively coupled plasma atomic emission spectroscopy (Spectro Modula, Germany). Chl *a* was determined by the fluorometric method [Holm-Hansen et al., 1965], and with high-performance liquid chromatography (HPLC) analysis, after extraction in Acetone 90% for 24 h. For ADRIA02 cruise, the in situ

fluorescence was converted into chlorophyll *a* units using the linear regression from the data ($n = 122$; $r = 0.897$; $P < 0.001$).

[22] Abundance, biomass and species composition of nanophytoplankton (between 2 and $20 \mu\text{m}$ as maximum linear dimension) and microphytoplankton (between $20 \mu\text{m}$ and $200 \mu\text{m}$) were estimated on 17 stations along four transects located south of Po delta; discrete samples were also gathered at 3 depths along the water column (surface, intermediate, and near-bottom layers). Samples were fixed with exometilentetramine-neutralized formaldehyde to a final concentration of 4% and examined after Utermöhl [1958] and Zingone et al. [1990]. Species composition was defined according to Tomas [1997]. The cells belonging to cryptophyceans, crysophyceans, prymnesiophyceans (except coccolithophorids), prasinophyceans, and chlorophyceans, whose sizes vary between 3 and $4 \mu\text{m}$ and remained undetermined, were all included in the group “nanoflagellates.” Cell size and volume were determined according to Strathmann [1967] and the phytoplankton carbon was obtained by multiplying cell or plasma volume by 0.11 for diatoms, coccolithophorids and nanoflagellates and by 0.13 for thecate dinoflagellates [Smetacek, 1975].

3. Results

3.1. Meteorological Conditions

[23] During the study period (16 September to 7 October 2002) the meteorological conditions were characterized by three episodes in which NE bora winds reached speeds larger than 10 m s^{-1} (Figure 2). Two episodes lasting 1 day

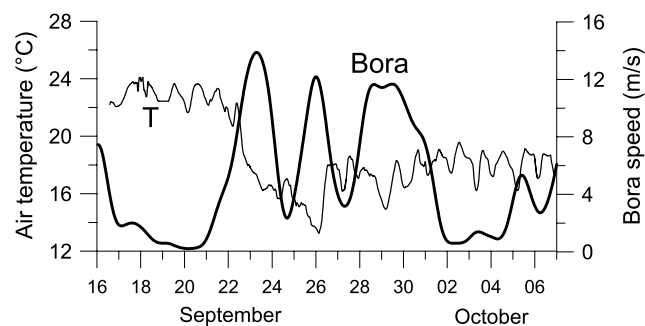


Figure 2. Air temperature (T) measured by the meteorological station on board R/V *Alliance* during the cruise is low-pass filtered, and maximum wind speed from NE (bora) just offshore of Istria is from COAMPS model.

were registered during 22–23 September and 25–26 September and the last one, occurred between 28 and 30 September, lasting almost 3 days. Despite these bora events were actually different in terms of pulsing and spatial structure, COAMPS model results have shown to successfully describe the wind situations during the period.

[24] The wind stress, as resulting from meteorological model (Figure 3), is northeasterly in nearly the whole NA basin, exhibiting the classical bora lineaments of these cold and katabatic winds, even if in some cases they may depart from that orientation while approaching the Italian coast (e.g., the case on 26 September). During the period between 23 and 28 September, the regions of higher wind intensity progressively move to the south while days are passing, showing a intensity maximum located in southern of Istrian peninsula on 28 September (Figure 3).

[25] The bora events were associated with increasing barometric pressure, following the passage of an atmospheric depression over the Adriatic Sea, consistent with previous bora analysis [Krajcar, 2003]. During the observed period, the air temperature dropped from 24.0°C to 12.9°C in 4 days with a decrease of about 2.8°C d⁻¹ (Figure 2).

3.2. Oceanographic Conditions: Modeling Results

3.2.1. Prebora Condition

[26] The simulated ROMS surface circulation and sea surface temperature (SST) fields are presented in Figure 4. During 17–18 September, the average wind stress is rather low, with winds generally directed from S-SW to N. The SST field is nearly homogenous, and the circulation indicates a weak counterclockwise gyre in the northern part of the basin, while a second gyre is evident north of Ancona (Figure 4a). The upper flow is clearly moving northward along the Croatian coast, and southward along the Italian coast. In the vicinity of the Po delta, the influence of the river discharge modified the upper flow, pushing the upper circulation to the center of the basin.

[27] At the bottom (Figure 4d), the magnitude of currents is much decreased and the sharpness of the counterclockwise gyres much attenuated. Bottom temperatures are higher in the coastal areas of the Italian side. Indeed, considering the difference between surface and bottom temperature (Figure 4g), there exists a narrow coastal band where salty bottom waters are generally warmer than fresh surface ones. Thermal inversion is present along the western coast and partially in the gulf of Trieste region, while it does not seem to hold in the Croatian areas. In the middle of the NA, however, the bottom waters are colder than the surface waters. Consequently, the coastal regions of the NA presents a shallow (inverted) thermocline (and halocline) mostly stratified, with the exception of the Croatian coast, where the water column appears to be mixed until most of the depths.

3.2.2. Condition During Bora

[28] As we previously said, the winds that characterized the observed period had a pulsing and spatially varying behavior; for instance, the first intense event during 22–24 September was not clearly setting up a gyre in the NA basin because of its spatial structure. As a period indicative of bora situation, we focus therefore on 25–28 September, in which the winds were northeasterly in nearly the whole basin, with a maximum located southern of Istria (Figure 3).

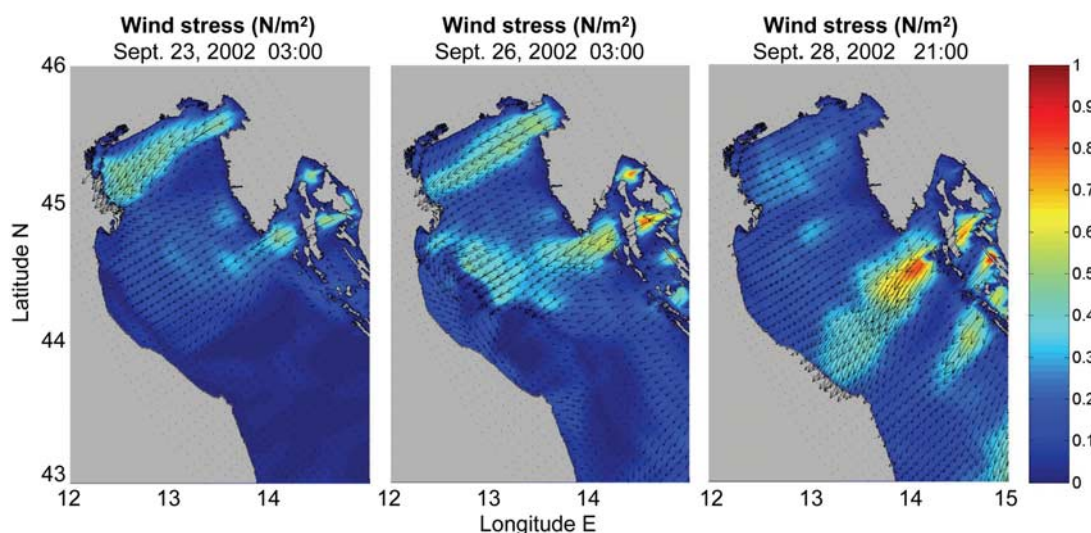


Figure 3. Wind stress (magnitude in N m⁻² and direction) from the COAMPS meteorological model on 23, 26, and 28 September 2002 during the higher bora peaks.

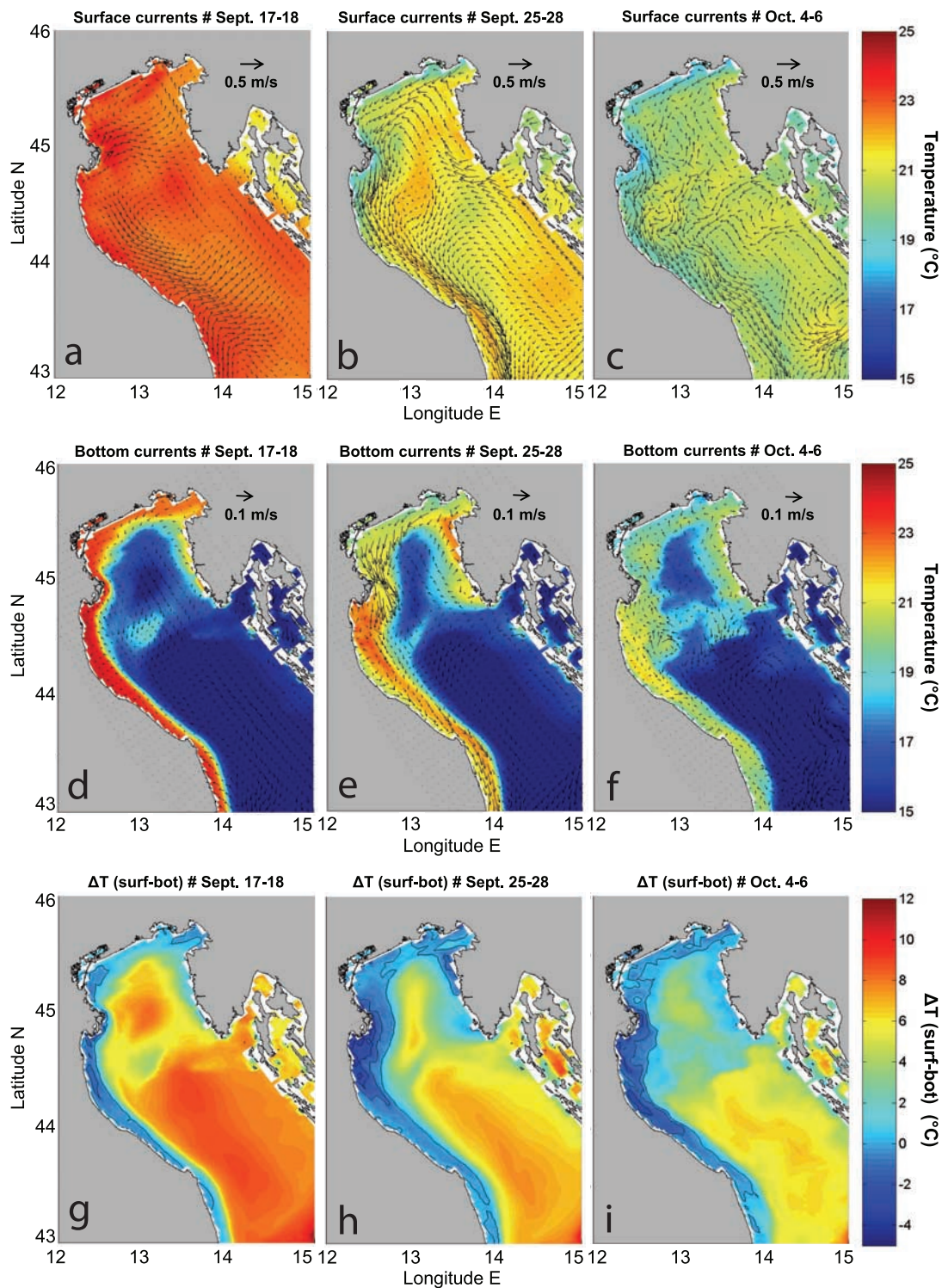


Figure 4. ROMS model results: (a, b, c) current vectors at surface and SST, (d, e, f) current vectors and temperature at bottom, and (g, h, i) ΔT surface-bottom temperature difference before bora (Figures 4a, 4d, and 4g), during bora (Figures 4b, 4e, and 4h), and after bora (Figures 4c, 4f, and 4i). Current is in m s^{-1} , and temperature is in $^{\circ}\text{C}$.

[29] The resulting average flow (Figure 4b) is now much more intense; an intense WACC is found along the whole western coast, and from Kvarner Bay currents are directed mainly toward the Italian coast (SW) with a secondary branch directed northwestward. Under the influence of the

strong winds that are increasing, current speeds at the surface increase up to 0.5 m s^{-1} . SST has clearly decreased, with cooler water along the Italian coast (now down to 19°C) and in the Croatian island region. During bora episodes, strong bottom currents are also found in the

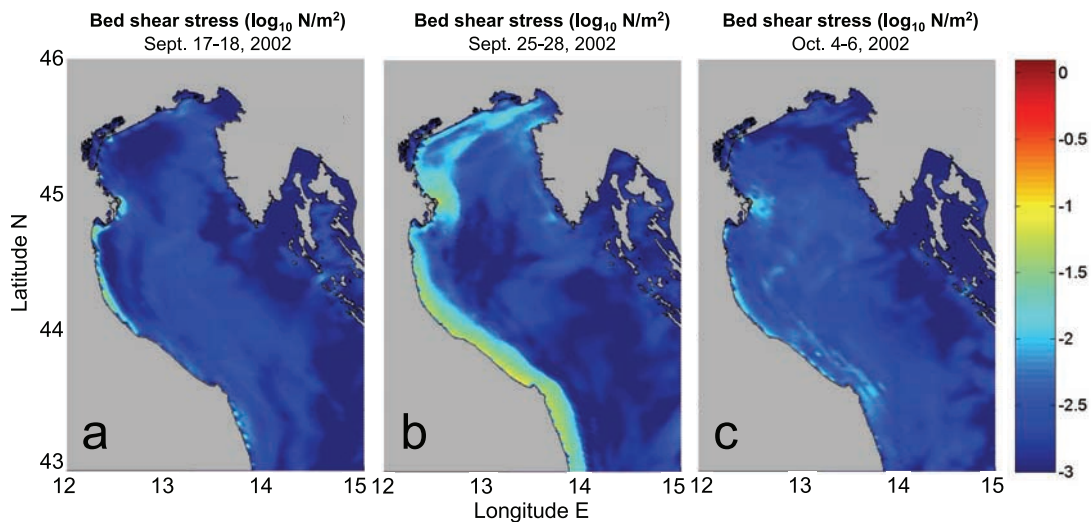


Figure 5. The log distribution of the bed shear stress ($\log_{10} \text{N m}^{-2}$) induced by the current-wave interactions in proximity of the bottom from model. Daily averages of (a) 17–18 September, (b) 25–28 September, and (c) 4–6 October.

WACC region (Figure 4e), with values typically around 0.1 m s^{-1} in the coastal region up to a depth of about 20–30 m. The flow is again generally south directed, with relative maxima (up to 0.25 m s^{-1}) in front of the Po delta. Bottom temperatures along the western coast show a general decrease, while offshore a general increase is detectable; this is an effect of the bora-enhanced mixing between surface and bottom waters. The surface/bottom temperature difference (Figure 4h) is now showing much larger regions close to the coast where the surface temperatures are lower than the bottom ones, clearly accounting for the cooling effect (by means of partial vertical mixing, as discussed later on) of the bora winds blowing over the basin. The large positive core that was characterizing the NA is now reduced to a small region in the middle of the basin. The mixed layer depth (not shown) is now much deeper in the northern basin, including the Po delta region, after the bora passage that homogenized the water structure. Another region where the depth of the mixed layer increased is in the central Adriatic, toward Ancona, closer to the coast. Here the effect of the cold wind has again mixed the vertical stratification that was present around 18 September.

3.2.3. Postbora Condition

[30] After 1 October, the wind stress becomes again moderate over the basin, leading to a surface circulation pattern that is now transitioning and relaxing from structures typical of the bora situation to those associated to weaker surface forcings. The SST has decreased (Figure 4c), mainly in response to vertical mixing induced by wind forcing as discussed later on. Despite being less coherent and less attached to the coast, the flow along the Italian coast is still energetic (surface currents up to 0.3 m s^{-1}), while the flow along the northern coast is now less pronounced and weaker. Bottom currents show a significant reduction in magnitude (Figure 4f), with values well below 0.1 m s^{-1} in the coastal regions, very close to the values of the prebora situation. The surface/bottom temperature difference (Figure 4i) still shows a rather large coastal band where the bottom values are larger than the surface ones; compared to the prebora situation, the

band is broader and includes all the Italian coasts. In the core of the NA basin the difference is now diminished (from 10°C prebora to $6\text{--}7^\circ\text{C}$ postbora). The basin is undergoing again a progressive (salinity driven) stratification, with the winds now absent or considerably decreased and the shallow pycnocline found in all the northern and western coastal regions extending offshore, resembling the prebora situation.

3.2.4. Bed Shear Stress

[31] The modeled distribution of bed shear stress is presented in Figure 5. In the period 17–18 September, low values of stress reflect a relatively calm situation, when low amounts of energy from the atmosphere are injected in the water column and redistributed to the bottom (Figure 5a). During the most intense bora event, the winds not only redistributed the heat and modified the surface currents, but also affected the bottom layers as well. Indeed, values of the bed shear stress in the order of (\log_{10}) between -1 and -2 , that before were present in very limited nearshore regions, are now extending well in the offshore direction up to 30–35 m depth, affecting the whole Italian coast with maxima around and south of the Po delta (Figure 5b). In the postbora period the averaged bed shear stress is again weaker, yet there exist regions where the bottom signature of the stress is significant, e.g., in front of the Po delta area and to its south (Figure 5c).

3.3. Oceanographic Conditions: Experimental Observations

3.3.1. Hydrology

[32] The SST measured during the experimental cruises, shows a quite homogeneous distribution at the beginning of the observation period (average $22.7 \pm 0.4^\circ\text{C}$, range $21.7\text{--}23.7^\circ\text{C}$; Figure 6a), and a progressive decrease to an average $20.3 \pm 0.6^\circ\text{C}$ at end of the observing periods (Figure 6b). The colder waters are soon confined to the shallow northern and western sides of the basin, creating a frontal system along the Italian coast particularly evident after 30 September. These patterns are in large part consistent with the results obtained from the hydrodynamic model

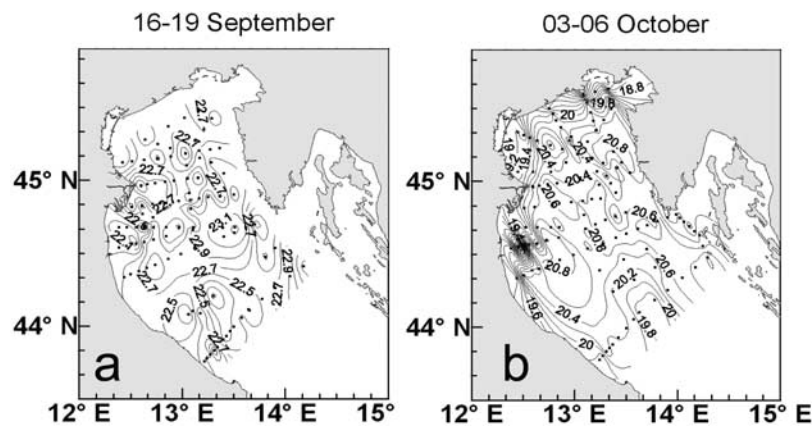


Figure 6. Distribution of temperature ($^{\circ}\text{C}$) at surface (a) before and (b) after bora events, measured during the oceanographic cruises.

simulations. At bottom significant variations in temperature were not observed during the period ($17.1 \pm 2.8^{\circ}\text{C}$ and $17.9 \pm 2.1^{\circ}\text{C}$ before and after bora event, respectively).

[33] Before the bora, low-salinity water, mainly outflowing from the Po River, extends both eastward and southward, occupying a large portion of the basin (Figure 7a) and developing a counterclockwise gyre structure as also depicted by the modeling results. The action of the bora wind confines the low-salinity water in the western coastal zone, while high-salinity waters (>38) from the eastern side occupied large part of basin (Figure 7b). The SST coastal front is also evident in a salinity signature, and at the end of observation period the diluted Po waters were confined in the western coastal area. The bottom waters had a minimum salinity (35.5) in the western coastal waters, with increasing values toward the southeast (up to 38.7). A general increase in the bottom salinity following the bora event was consistent with the inflow of high-salinity waters from the south along the Istrian peninsula, balancing the outflow of water from the NA along the Italian coast. Maximum observed densities (γ_{θ}) were 27.6 kg m^{-3} at surface and 29.2 kg m^{-3} at bottom. The bora blew cooling down the water and deepening the halocline but the wind stress caused a mixing in the upper part of water column, up to about 20–25 m depth; the mixing did not reach the bottom in the deeper

part of basin, as evidenced by the variations of density profiles along the water column in center of basin (station VR04, 33 m depth) during the observing period (Figure 8).

3.3.2. Dissolved Oxygen and Inorganic Nutrients

[34] In order to analyze the basin distribution pattern of the dissolved oxygen saturation (DO) and nutrient concentrations, together with hydrologic parameters, quantities were averaged and grouped into three different water types and three different periods (16–19 September before, 27–29 September during, and 30 September to 5 October after the event; see Table 1). The water types were differentiated according to their salinity (S) and DO as (1) type 1, surface diluted waters ($S < 38$; $\text{DO} \geq 90\%$); (2) type 2, other surface waters ($S \geq 38$; $\text{DO} \geq 90\%$); and (3) type 3, undersaturated deep waters ($S \geq 38$; $\text{DO} < 90\%$).

[35] DO at the surface is close to saturation in the whole basin (average 102–103%), and shows a marked increase in time, reaching values over 125% in the diluted western coastal waters after the bora event. In the deeper part of the NA the bottom waters are generally undersaturated at the beginning of observing period and a wide area with stronger hypoxic conditions (DO minimum value 26%) is located south of Po delta, near the isobaths of 30 m, extending toward the Istrian peninsula (Figure 9a). Since the mixing occurred only in the upper part of water column, complete

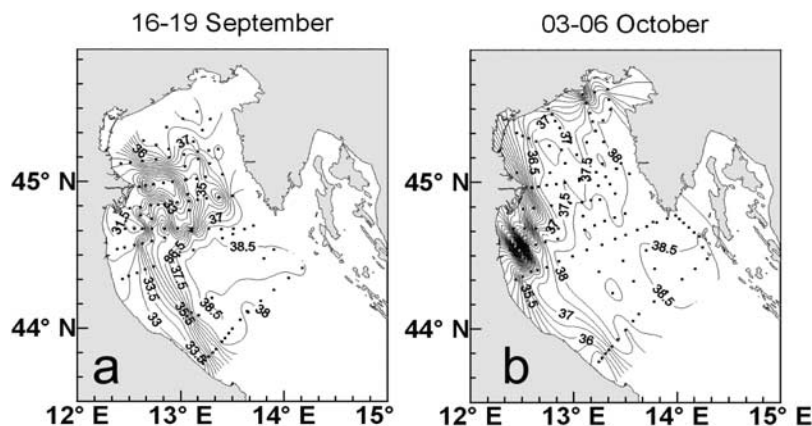


Figure 7. Distribution of salinity at surface (a) before and (b) after bora events, measured during the oceanographic cruises.

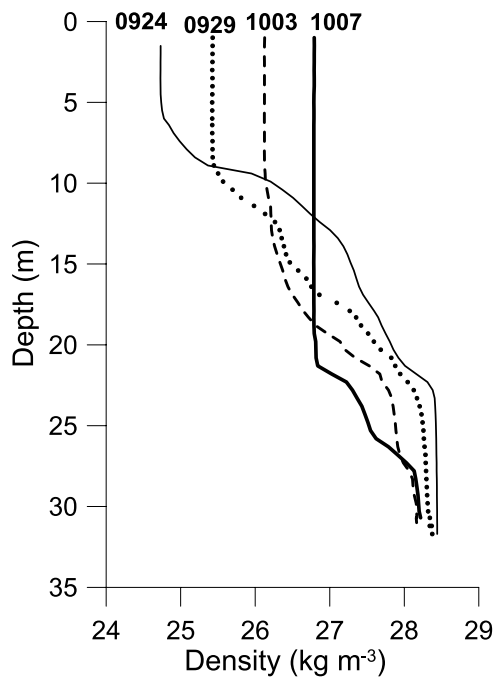


Figure 8. Vertical density profiles in station VR04 in center of NA basin (see Figure 1 for location) during the observing period on 24 September (thin line), 29 September (dotted line), 3 October (dashed line), and 7 October (thick line).

oxygenation was observed down to the bottom only in the coastal area and in the westernmost stations DO increased at the bottom from 50% to 90%. In the deeper central area, hypoxic conditions were maintained throughout the whole study period, although showing a increase in saturation values and a limited spatial shifting (Figure 9a).

[36] For dissolved inorganic nutrients, higher concentrations are generally found in type 3 deep water, with the exception of nitrate (NO_3), which is higher in the low-salinity water (type 1; Table 1). During 16–19 September the prevailing nitrogen form in the high-salinity waters (types 2 and 3) is ammonia (on average 53–65% of DIN; Table 1). Higher values for nitrites and orthosilicates are present in central bottom waters (Figures 9b and 9c), approximately coincident with the lower-DO area.

[37] South of the Po delta the nitrate is higher in the low-salinity surface layer ($\text{NO}_3 > 2 \mu\text{M}$) while for orthosilicates the maximum values (up to $21.4 \mu\text{M}$) are reached at the bottom, along the Italian slope, as highlighted in the Cesenatico-Pula transect in particular during and after the bora events (Figure 10). The dissolved nitrogen was mainly present in reduced forms as evidenced by the lower nitrate:ammonia ratio at the bottom (averaged $\text{NO}_3/\text{NH}_4 = 0.6$).

[38] During and after the bora event, in the low-salinity water confined to a narrow band along the Italian coast, a general increase of nutrients concentration was observed, particularly evident in NO_3 and $\text{Si}(\text{OH})_4$ in Cesenatico-Pula transect (Figure 10). At the same time, a decrease in

Table 1. Hydrologic Properties, DO, and Nutrients of Different Water Types in Three Periods^a

Parameters	16–19 September			27–29 September			30 September to 5 October		
	n	Average	SD	n	Average	SD	n	Average	SD
<i>Type 1 ($S < 38$; $DO \geq 90\%$)</i>									
Temperature ($^{\circ}\text{C}$)	-	23.2	0.6	-	21.1	0.6	-	20.8	0.5
Salinity	-	36.2	1.8	-	37.2	0.9	-	37.2	1.0
Density (kg m^{-3})	-	24.8	1.3	-	26.1	0.6	-	26.2	0.7
DO (%)	31	102	7	40	103	3	74	107	13
NO_3 (μM)	31	2.3	4.5	39	1.8	1.8	74	2.7	5.3
NO_2 (μM)	31	0.2	0.1	39	0.3	0.4	74	0.3	0.4
NH_4 (μM)	31	1.9	1.7	39	1.5	1.7	74	1.2	1.4
$\text{Si}(\text{OH})_4$ (μM)	31	5.8	4.7	39	4.6	3.9	74	5.1	5.1
PO_4 (μM)	31	0.07	0.03	39	0.06	0.03	74	0.05	0.03
<i>Type 2 ($S \geq 38$; $DO \geq 90\%$)</i>									
Temperature ($^{\circ}\text{C}$)	-	20.4	3.1	-	19.6	2.5	-	19.3	2.1
Salinity	-	38.4	0.2	-	38.4	0.2	-	38.4	0.2
Density (kg m^{-3})	-	27.2	4.2	-	27.5	0.8	-	27.6	0.7
DO (%)	51	103	4	35	103	5	49	102	4
NO_3 (μM)	51	1.0	0.6	33	0.8	0.8	49	0.9	0.6
NO_2 (μM)	51	0.1	0.1	33	0.2	0.1	49	0.3	0.4
NH_4 (μM)	51	2.1	1.8	33	1.5	2.1	49	1.2	1.6
$\text{Si}(\text{OH})_4$ (μM)	51	5.5	2.7	33	4.3	2.6	49	4.7	4.2
PO_4 (μM)	51	0.09	0.04	33	0.05	0.03	49	0.05	0.03
<i>Type 3 ($S \geq 38$; $DO < 90\%$)</i>									
Temperature ($^{\circ}\text{C}$)	-	17.0	3.1	-	16.9	2.86	-	17.2	1.4
Salinity	-	38.4	0.1	-	38.4	0.13	-	38.4	0.1
Density (kg m^{-3})	-	28.1	0.8	-	28.1	0.80	-	28.1	0.3
DO (%)	31	71	15	20	72	14	25	63	18
NO_3 (μM)	31	1.6	0.8	16	1.5	1.3	25	1.7	1.9
NO_2 (μM)	31	0.8	0.7	16	0.9	1.4	25	1.9	1.4
NH_4 (μM)	31	2.8	1.6	16	1.3	1.0	25	1.8	2.2
$\text{Si}(\text{OH})_4$ (μM)	31	14.8	6.3	16	15.2	8.2	25	17.1	7.2
PO_4 (μM)	31	0.11	0.07	16	0.10	0.06	25	0.10	0.06

^aSD, standard deviation; n, number of observations. The different water types identify different waters: diluted-surface waters (type 1), offshore surface water (type 2), and offshore bottom water (type 3). The numbers of observations are not reported for hydrologic parameters, obtained from CTD vertical continuous profiles.

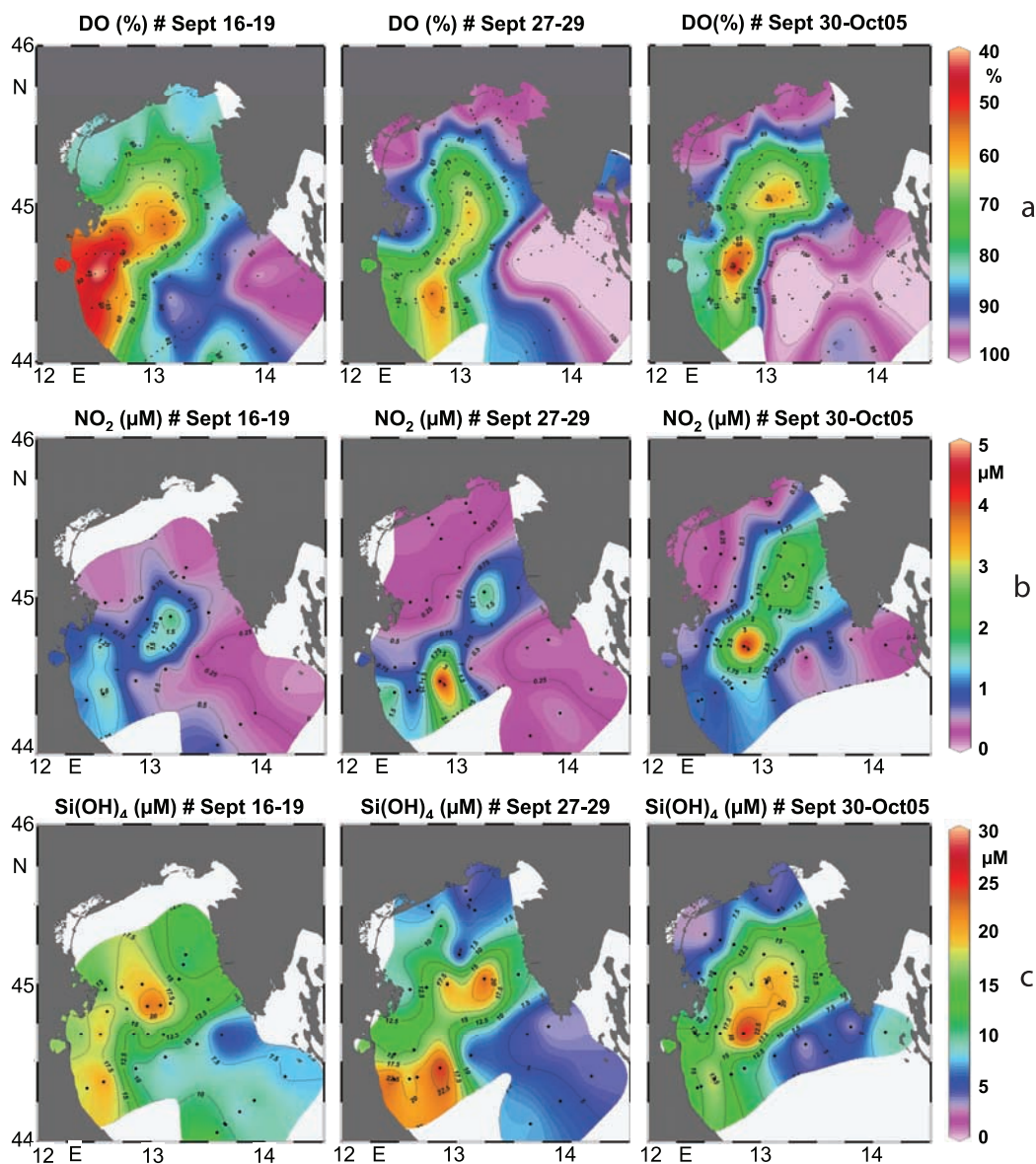


Figure 9. Distribution of (a) dissolved oxygen (DO in percent saturation), (b) nitrites (NO_2 in μM), and (c) orthosilicates ($\text{Si}(\text{OH})_4$ in μM) during 16–19 September, 27–29 September, and 30 September to 5 October (plots realized by Ocean Data View program [Schlitzer, 2002]).

nutrients in the central part of transect is likely due to the inflow of more oligotrophic waters from the east as showed by the increasing salinity (Figures 7 and 10) and, down to 25 m depth in the well mixed layer, water is lower in nutrient concentrations ($\text{NO}_3 < 1 \mu\text{M}$, $\text{Si}(\text{OH})_4 < 5 \mu\text{M}$).

[39] At bottom, nitrates and nitrites constantly increase in time, being initially 46% of DIN, going up to more than 65% of DIN at the end of observing period. NO_2 and $\text{Si}(\text{OH})_4$ distributions and time variations show this increasing trend (Figures 9b and 9c), whereas the PO_4 concentration shows a contrary decreasing trend. In the same time, ammonia decrease to about 30% of DIN and the NO_3/NH_4 ratio increase to 1.0–1.2. The noticeable feature is represented by the highest values at bottom on the Italian slope

both for NO_3 (up to $9.1 \mu\text{M}$) and $\text{Si}(\text{OH})_4$ (more than $30 \mu\text{M}$; Figure 10).

3.3.3. Suspended Matter and Chlorophyll

[40] The average concentration and composition of suspended matter in three water types for the periods 27–29 September and 30 September to 2 October are reported in Table 2. The concentrations of total suspended matter, particulate organic carbon, particulate nitrogen, and total particulate phosphorus fall within the same range of those reported for different water masses in the NA [Gismondi *et al.*, 2002].

[41] During the bora event, average TSM concentration in the western coastal area, at surface, is 2.5 mg L^{-1} , whereas in the eastern area it is lower than 0.5 mg L^{-1} (Figure 11, top). Higher TSM concentration appears

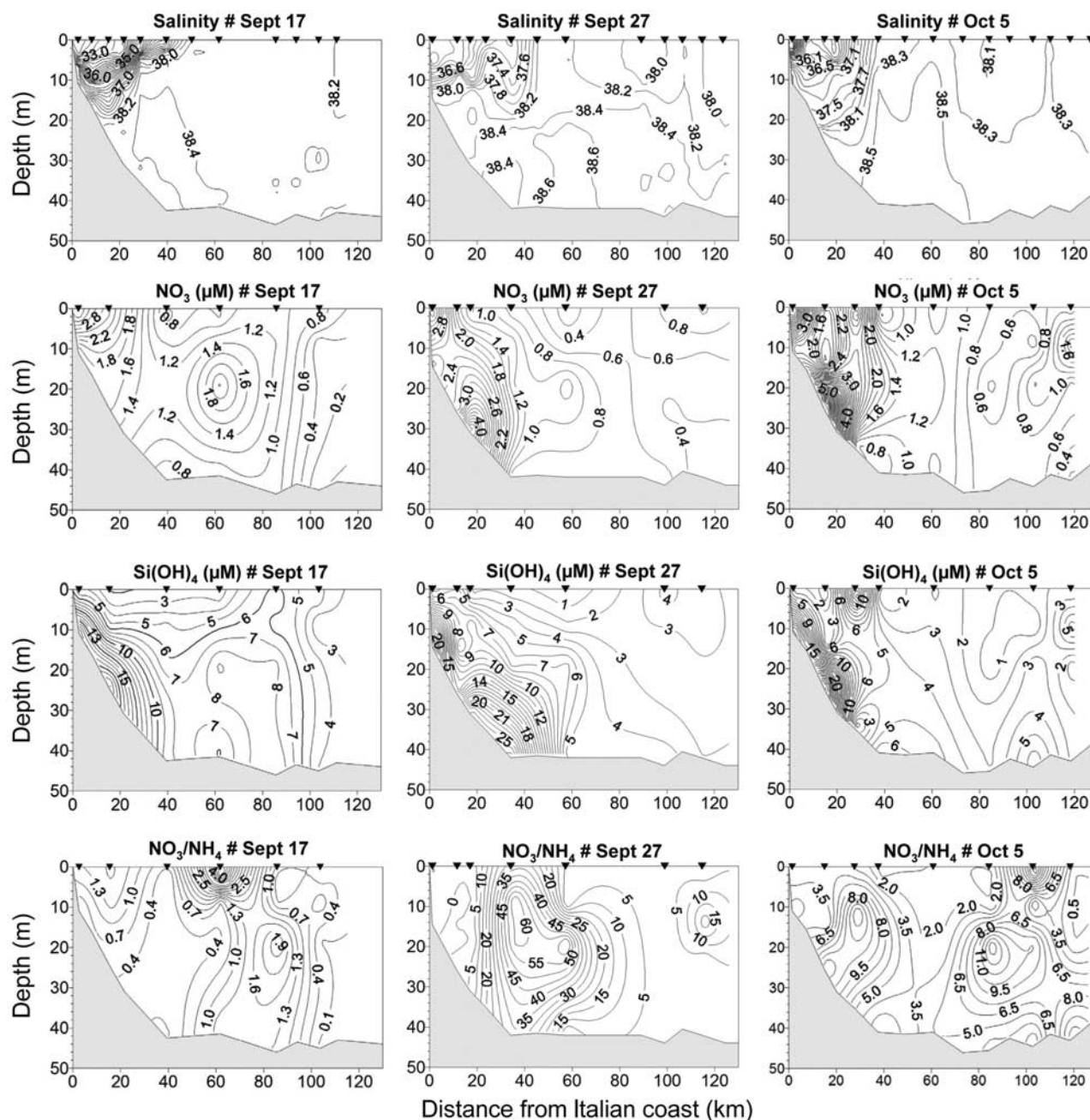


Figure 10. Distribution of salinity, nitrate (contour interval is $0.2 \mu\text{M}$), orthosilicate (contour interval is $1 \mu\text{M}$), and nitrate/ammonia ratio along the Cesenatico-Pula transect on 17 September, 27 September, and 5 October.

correlated with the spreading of diluted water in the basin (see salinity distribution at surface; Figure 7). At the bottom, TSM increased progressively in the western side of the basin and the region with concentrations larger than 2.5 mg L^{-1} expanded to water depths up to 30–35 m (Figure 11, bottom), and this seems related to the area characterized by higher bed shear stress during the bora, evidenced in the models results (Figure 5).

[42] Particulate organic matter (as POC, PTN, and TPP concentrations) showed a decreasing pattern from the coast to the offshore waters, with intermediate values in the bottom waters (Table 2). The particulate organic matter was 2–3 times higher in the low-salinity oxygen-supersaturated

waters than in the high-salinity waters. At the surface, both for diluted and offshore waters, organic fractions increased with time, a trend more evident in the offshore waters (e. g. the organic carbon content of suspended matter increased from 6.5% to 13.9% of TSM). In deep waters, the increase of TSM in time was not followed by a similar increase in the organic fraction; average values of organic carbon content were similar in the two periods considered (POC 3.9% and 3.2% of TSM), showing that suspended matter in the bottom layers probably has the same source throughout the study period. The lower content of organic carbon in the particulate matter of deep waters can be attributed to degradation of organic matter in

Table 2. Suspended Matter Characteristics and Biogeochemical Composition in Water Types 1, 2, and 3 in Two Periods

Parameters	27–29 September			30 September to 2 October		
	n	Average	SD	n	Average	SD
<i>Type 1 ($S \leq 38$; $DO \geq 90\%$)</i>						
TSM (mg L^{-1})	39	2.5	2.7	43	2.0	1.6
POC (μM)	39	19.0	8.4	25	19.0	9.5
TPN (μM)	39	2.5	1.1	25	3.0	1.7
TPP (μM)	36	0.07	0.06	15	0.11	0.11
C/N (mol/mol)	39	7.8	1.3	28	6.7	0.9
POC/TSM (%)	39	16.3	13.0	27	19.4	19.0
Chl <i>a</i> ($\mu\text{g L}^{-1}$)	39	1.7	1.3	22	2.0	1.6
<i>Type 2 ($S > 38$; $DO \geq 90\%$)</i>						
TSM (mg L^{-1})	33	1.5	0.9	15	1.1	0.5
POC (μM)	33	5.7	2.3	7	10.0	5.0
TPN (μM)	33	0.8	0.4	7	1.5	0.5
TPP (μM)	32	0.03	0.02	2	0.04	0.02
C/N (mol/mol)	33	6.9	1.0	7	6.4	1.1
POC/TSM (%)	33	6.5	7.1	7	13.9	12.0
Chl <i>a</i> ($\mu\text{g L}^{-1}$)	33	0.6	0.6	5	0.9	0.6
<i>Type 3 ($S > 38$; $DO < 90\%$)</i>						
TSM (mg L^{-1})	16	3.4	3.0	5	3.5	1.4
POC (μM)	16	7.8	2.6	5	8.8	2.2
TPN (μM)	16	1.2	0.5	5	1.5	0.5
TPP (μM)	16	0.08	0.04	3	0.11	0.05
C/N (mol/mol)	16	6.6	0.9	5	5.9	0.4
POC/TSM (%)	16	3.9	2.3	5	3.2	0.6
Chl <i>a</i> ($\mu\text{g L}^{-1}$)	16	0.8	0.6	5	0.8	0.3

water column and/or to the resuspension of bottom sediments, which are characterized by an organic carbon content between 0.44 and 1.24% (as reported for the Po delta area by *Miserocchi et al.* [2007]).

[43] Before the wind blows, high Chl *a* concentrations at the surface followed the low-salinity distribution pattern (Figure 12). During the bora events, Chl *a* concentrations progressively dropped to values less than $0.5 \mu\text{g L}^{-1}$ in the whole basin, and higher values were present only along the western coast. After the bora events, in wind calm situation, a general increase of phytoplankton pigments was observed in the basin (Figure 12 and averaged values in Table 2), reaching the highest concentrations in the western area south of Po delta.

3.3.4. Space and Time Variability of the Phytoplankton Biomass and Composition

[44] A decreasing gradient of abundance and biomass of phytoplankton was generally observed from west to east, moving from low-salinity waters to offshore. The abundance decreased from $1.8 \cdot 10^6$ to $0.4 \cdot 10^6 \text{ cell L}^{-1}$, and the biomass from 75.2 to $16.1 \mu\text{g C L}^{-1}$. The nanophytoplankton constituted the dominant fraction in abundance (on average 72%), while the microphytoplankton contribution was 28%. In carbon biomass, the nanophytoplankton fraction contributed in average with 44% and the microphytoplankton with 56%.

[45] The dominance of diatoms (mean abundance and biomass contribution of 66% and 83%, respectively) and

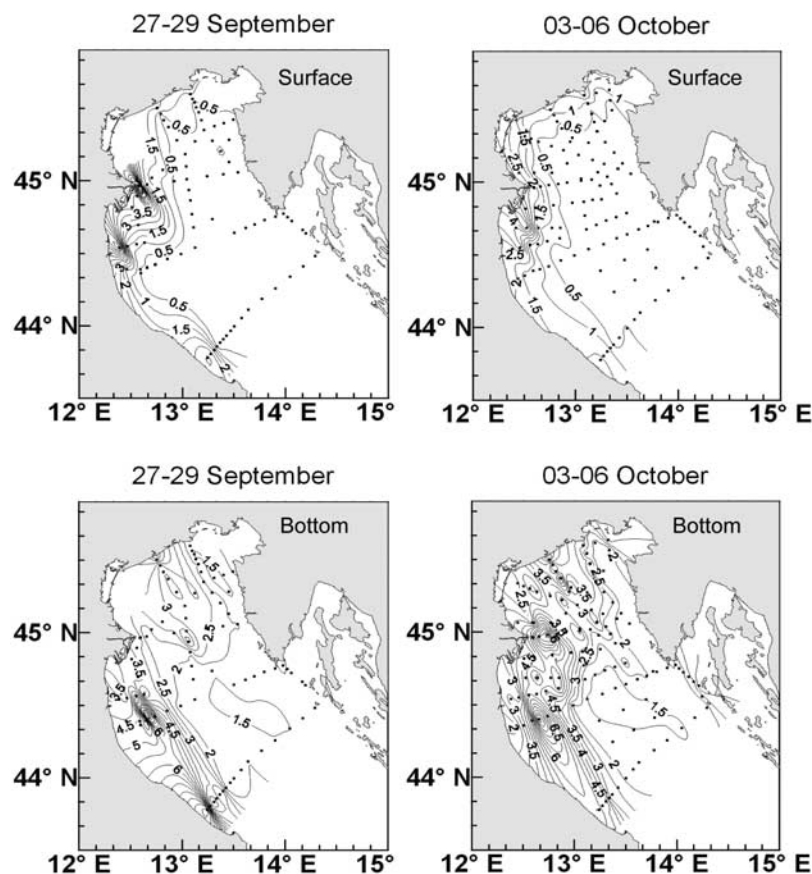


Figure 11. Turbidity as TSM (mg L^{-1}) (top) at surface and (bottom) at bottom during the bora event (27–29 September) and after the event (3–6 October).

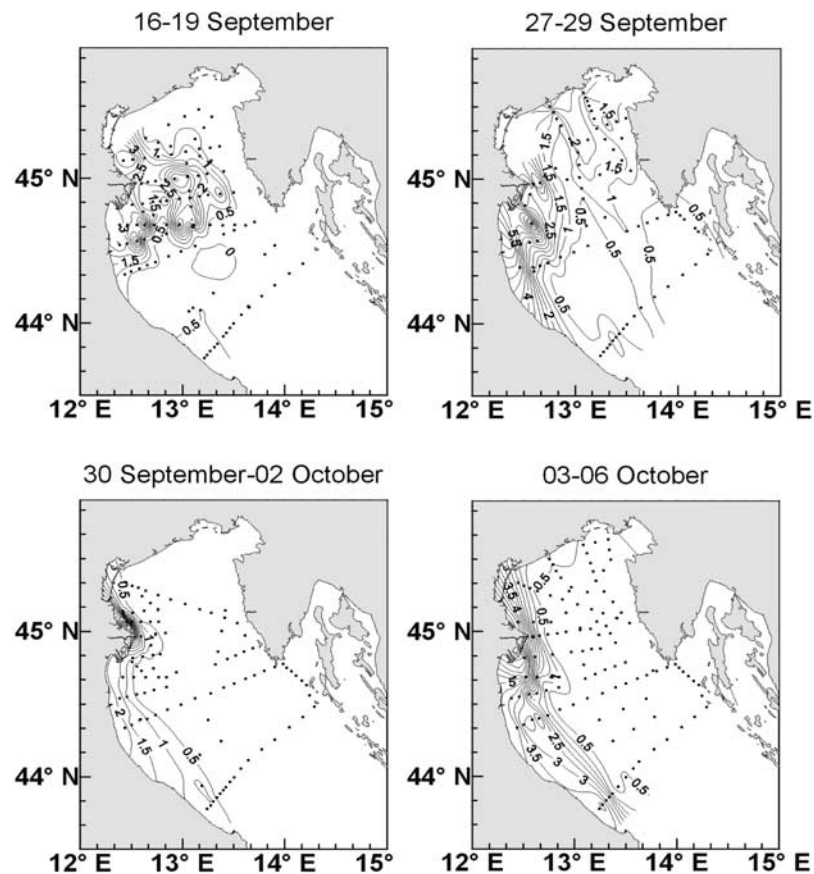


Figure 12. Surface data of in situ fluorescence in four time intervals (16–19 September, 27–29 September, 30 September to 2 October, and 3–6 October) in arbitrary units for the first period (16–19 September) and in Chl *a* ($\mu\text{g L}^{-1}$) for others.

nanoflagellates (30% and 3%) characterized the community without qualitative differences among the stations. Dinoflagellates (mean abundance and biomass contribution of 3% and 9%, respectively) and coccolithophorids (1% and 5%) presence was limited mainly in the eastern stations or near the bottom. The species belonged to a late summer community reported for the northwestern Adriatic Sea [Socal and Bianchi, 1989; Socal et al., 1992; Bernardi Aubry et al., 2004; Totti et al., 2005], characterized by a rich community of diatoms mainly represented by *Chaetoceros* spp., *Cerataulina pelagica*, *Pseudo-nitzschia delicatissima* complex and dinoflagellates (mainly *Gymnodinium* spp.). After the bora events, a relevant peak of phytoplankton abundance and biomass (values $9.4 \cdot 10^6 \text{ cell L}^{-1}$ and $371.8 \mu\text{g C L}^{-1}$, at surface) was developed southwest of the Po delta, as response to the nutrients increase. In this situation diatoms (mainly *Chaetoceros* spp. and *Cerataulina pelagica*) represented the dominant group with a contribution of 90% of abundance and carbon biomass.

4. Discussion

4.1. Suspended Sediment and Transport Processes in Response to the Bora

[46] Bora winds are most common during the cool season (November to March), and in Trieste the highest frequency of occurrence and strongest winds are from December to

February. Here the average duration of a gale-force ($>15 \text{ m s}^{-1}$) bora varies from 3 days in winter to 1 day in summer [Poulain and Raicich, 2001]. Bignami et al. [2007] provided histograms with the monthly number of days and the daily Adriatic Sea average wind speeds for the Bora winds; it turned out that Bora winds were the only ones that generally abate in April–August, and then resume in September, with higher winds in colder months. Lukšić [1975] showed that for Senj, the station in Croatian coast where the bora usually attains the greatest speeds, the wintertime bora typically lasts 1 day but may in some cases extend over more than 10 days, and that the maximum speeds may surpass 40 m s^{-1} . Bora blowing is characterized by a relevant variability not only at diurnal, synoptic and seasonal time scale, but also at interannual and decadal ones. Pirazzoli and Tomasin [1999] evidenced a declining trend in frequency and strength of bora events in Trieste (but this conclusion cannot be extended to bora blowing from other gaps over the Adriatic Sea).

[47] The moderate bora events occurring in our study period are representative of the first relevant vertical mixing events of the fall, when the NA water column is stabilized by heat gained during the summer. The water column before the bora events was stratified, characterized by the presence of diluted waters spreading in large part of the basin and cold bottom waters in the central and eastern region. The mixing processes due to the bora caused a breakdown of the

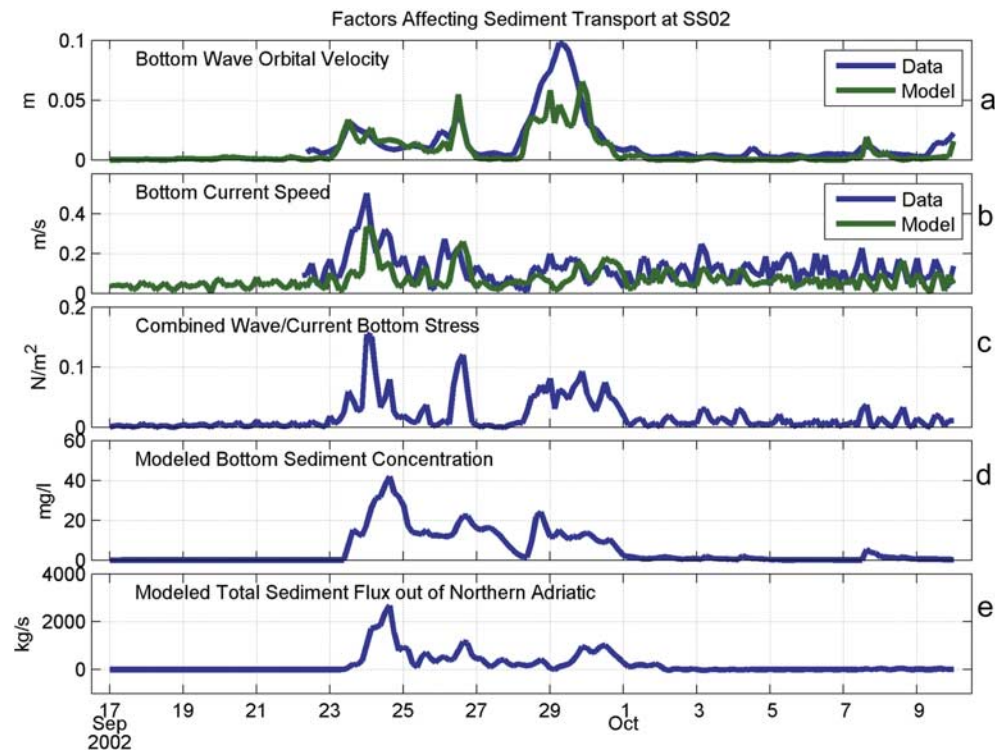


Figure 13. The factors affecting sediment transport and the influence of the bora during the study period at station SS02 (see Figure 1 for location), the site of an upward looking 300 kHz acoustic Doppler current profiler, located at 27 m water depth in the heart of WACC. It is evident that both the waves during 28 September to 1 October (Figure 13a) and the bottom current speeds during 23–27 September (Figure 13b) play important roles in contributing to the bottom stress (Figure 13c).

water stability in the upper layers. Noticeable features observed during and after the cold wind blowing are the mixing down to 20–25 m depth in the western area and the inflow of high-salinity water from the south along the Croatian coast. By analyzing the variation of the total heat content in the water column between the period 16–19 September and 3–6 October in the area between the Po delta and Istria, we verified that the heat loss was very limited, so the observed mixing was mostly due to the wind action, so the mixed layer depth evolution in the basin, progressively deepening and extending to both the west and east coasts, reflects the wind forcing acting on the sea surface. The wind mixing did not reach the bottom, as confirmed also by the persistence of oxygen hypoxic conditions in proximity of the bottom, and this can be due to the bora weakening in this area combined to the relatively strong salinity stratification, able to maintain a density gradient strong enough to limit the bora from completely mixing the water column [Beg Paklar *et al.*, 2001].

[48] Together with a net water transport directed to the west in upper part of the Adriatic, under the direct effect of the bora winds, the ROMS model results evidence a water transport that is directed also toward the Istria coast, immediately below the Po delta region. This was also evidenced and described in association with other bora situations by Bignami *et al.* [2007]. To the south of this circulation feature, another gyre appears, roughly bracketed between the region of strong bora blowing out of the Croatian region and the Ancona promontory.

[49] As wind blows across the surface of the sea it causes horizontal and vertical motions in the water. Bora, intensifying the alongshore western current in the same direction as the residual Adriatic cyclonic flow [Bergamasco and Gačić, 1996], influences the sediment distribution and transport [Fain *et al.*, 2007]. High sediment concentrations are associated with waves generated during bora events, and currents strengthening during these events drive sediments southward [Lee *et al.*, 2005].

[50] In terms of suspended matter concentration, the presence of benthic nepheloid layer (BNL) near the bottom on the slope (between 15 and 40 m) was substantially constant before and during the events. The sediment transport increased in relation to the winds and its magnitude and direction can be attributed to the interaction between the shallow bathymetry and wind-driven circulation described by Fain *et al.* [2007].

[51] To study the sediment transport in the period in relation with bora events, a time series of relevant parameters extracted from the model were analyzed for station SS02 (located in front of Senigallia; see Figure 1), and the results are presented in Figure 13. Station SS02 was selected because of the availability of experimental data for calibrating the model results. As described by Book *et al.* [2007], during ADRIA02 cruise several bottom-mounted acoustic Doppler current profilers were deployed by the U.S. Naval Research Laboratory (NRL) along the Senigallia-Susak line and station SS02 was the most westward station of the section, at a depth of about 25 m.

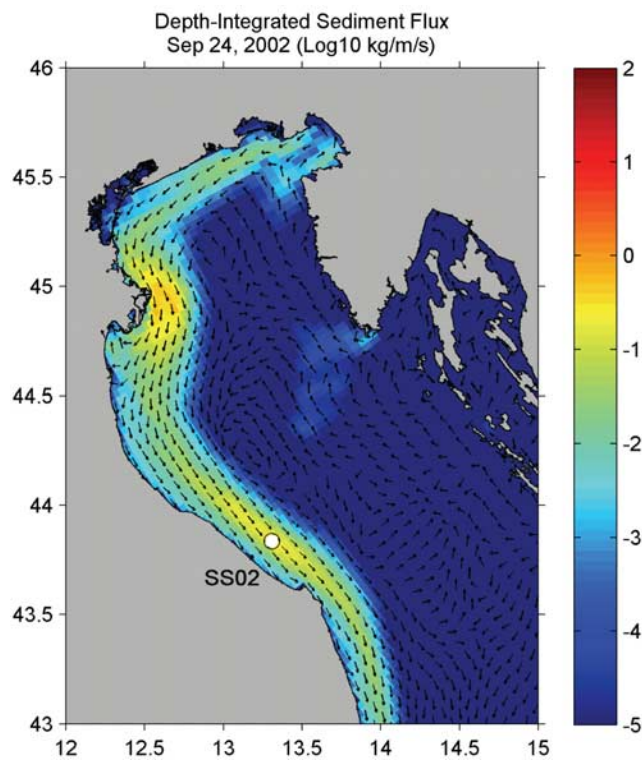


Figure 14. Depth-integrated sediment flux from the ROMS model during 24 September 2002, the peak of the sediment transport during the bora event. Station SS02 (white circle) is in the middle of the high-transport region (for clarity, every second point is shown).

[52] A good qualitative correlation between observed and modeled bottom wave orbital velocities (Figure 13a) and observed and modeled bottom currents (Figure 13b) in the examined period is evident. Moreover, there exists also a good correlation between the combined wave bottom stress and the bottom sediment concentration predicted by the model, indicating dominance of local resuspension in this region characterized by fine grain size of sediments [Brambati *et al.*, 1983]. Finally, there is a good correlation between the modeled sediment concentration and the total flux of sediment at SS02 during the intense wind events. This is likely because most sediments are fluxed out of the NA by the high-velocity bora-enhanced currents along the Italian coast.

[53] Extending the analysis in the whole basin, the daily averaged depth-integrated flux of sediments during 24 September, when the sediment transport was at its peak, is shown in Figure 14. Station SS02, from which time series were extracted and shown in Figure 13, is located in the middle of the high-transport region.

[54] Along the Italian coast, the flux is generally everywhere southeasterly directed, with largest values (more than $1 \text{ kg m}^{-1} \text{ s}^{-1}$, about $90 \text{ t m}^{-1} \text{ d}^{-1}$) found in proximity of the Po delta, and along the Italian coast. In the Gulf of Trieste there is an inflow and outflow. A small region of sediment transport is evident in the proximity of the southern Istria peninsula as well, where the bora effects are very intense. These situations of sediment flux southeasterly directed

appear to be associated with largest wavefields and a strengthening of the WACC along the Italian coast, a typical feature induced by intense bora episodes [Harris *et al.*, 2008]. These factors, together with the different grain size and shallower depths, are also explaining why in region of the western coast below 30 m the depth integrated sediment flux appears to be sensibly less. Along the Croatian coast, being waves and bottom currents much less developed, the sediment flux is only a few kilograms per meter per day.

[55] As it can be seen in Figure 13, the maximum flux of sediment out of the NA (Figure 13e), reached on 24 September, does not occur at the maximum bottom wave orbital velocity (Figure 13a). Indeed, it happens because the bottom currents were higher (Figure 13b), thus allowing the combined wave/current bottom stress to attain its maximum, around 0.13 N m^{-2} (Figure 13c), a peak that was responsible for sediment mobilization and transport. This is indicated also by the value of the modeled sediment concentration (Figure 13d).

4.2. Nutrient and Phytoplankton Dynamic in Response to Bora Wind

[56] As general pictures, the inorganic dissolved nutrient distribution shows an increasing concentration in the water column during and after the wind events (concentration of nitrate from 1 to $3 \mu\text{M}$ to $>4 \mu\text{M}$, orthosilicate from 4 to $5 \mu\text{M}$ to $>10 \mu\text{M}$).

[57] On the southwestern slope, the higher concentration in nutrients (mainly NO_3 and $\text{Si}(\text{OH})_4$) could be related to sediment mobilization induced by the increasing shear stress occurring mainly in this area, as evidenced by model simulations. The resuspension of bottom sediments could release reduced inorganic forms of nitrogen (e.g., nitrites, ammonia) which can then be oxidized in the water column. This would be consistent with the observed increase in NO_3/NH_4 ratio at the end of observation period, caused by the higher nitrate concentration due to oxidation processes.

[58] Higher bottom stress stimulates nitrification in the sediment and consequent release of nitrite and nitrate into the overlying water, as observed by Tengberg *et al.* [2003] with in situ experiments. In the same way, the increase in $\text{Si}(\text{OH})_4$ could be related to the increasing dissolution fluxes of biogenic opal due to the energetic conditions or/and by an enhanced diffusion upward from the sediment during the resuspension. The PO_4 showed the opposite trend, decreasing in time, that can be linked to the adsorption of phosphate to mineral particles such as iron oxides and the formation of iron oxide rich particles could be stimulated by resuspension [Tengberg *et al.*, 2003].

[59] At the beginning of observations, in stratified low-oxygenated water column, nitrogen was present at the bottom mostly as reduced forms (NO_2 and NH_4). The mixing process mainly due to the wind stress increased the oxygen saturation at bottom in the central area of the basin and this can determine the increase of $\text{NO}_3 + \text{NO}_2$ with respect to the previous calm weather situation. In this area a NH_4 decrease from 2.9 to $1.7 \mu\text{M}$ and a NO_2 increase from 0.7 to $1.1 \mu\text{M}$ in about 10 days were observed, whereas the NO_3 did not change appreciably (1.4 – $1.5 \mu\text{M}$). Even if the ammonia uptake into the bottom sediment seems a general process observed in the Adriatic Sea [Baric *et al.*, 2002], this was related mainly to sediment resuspen-

Table 3. Net and Southeastward Transports for DIN ($\text{NH}_4 + \text{NO}_2 + \text{NO}_3$), $\text{Si}(\text{OH})_4$, PO_4 , and Water Obtained in This Work^a

	During Bora Event on 27 September 2002 (Cesenatico-Pula Transect)	After Bora Event on 5 October 2002 (Cesenatico-Pula Transect)	Yearly Budget ^b (Northern Adriatic)
<i>Southeastward Flux</i>			
DIN (mol s^{-1})	355	233	128
$\text{Si}(\text{OH})_4$ (mol s^{-1})	750	319	322
PO_4 (mol s^{-1})	8.2	2.7	6.2
Water ($\text{m}^3 \text{s}^{-1}$)	110,691	86,570	100,000
<i>Net Flux (Positive Southeastward; Negative Northwestward)</i>			
DIN (mol s^{-1})	267	-35	75
$\text{Si}(\text{OH})_4$ (mol s^{-1})	495	-88	135
PO_4 (mol s^{-1})	5.3	-0.9	3.9
Water ($\text{m}^3 \text{s}^{-1}$)	53,887	2054	-

^aYearly estimations obtained by *Degobbi and Gilmartin* [1990] are reported as a reference.

^bFrom *Degobbi and Gilmartin* [1990].

sion [Simon, 1988]. In our case, the resuspension did not occurred intensively in the central area of basin, as evidenced by the bottom currents obtained by the model. Moreover, other observations indicate that the benthic flux have low relevance even in presence of resuspension processes [Tengberg *et al.*, 2003]. Then, the observed decrease of NH_4 and the parallel increase of NO_2 seem related to the importance of the chemical or microbial oxidative processes occurring in water column.

[60] Water masses with high concentration of NO_2 were already observed in NA [Solidoro *et al.*, 2007], and the rapid accumulation of nitrite in center of basin could be related to the relatively fast oxidation process from NH_4 to NO_2 and to a lag in the complete remineralization from ammonium to nitrate as observed by Socal *et al.* [2008]. Moreover, the slight increase of NO_3 concentrations with respect to NO_2 could be attributed to the biological consumption due to phytoplankton growth in calm wind as shown by the simultaneous increase in Chl *a*.

[61] The deeper part of basin with lower DO values was characterized by higher concentration of $\text{Si}(\text{OH})_4$, and this could be due to the releasing and remineralization processes occurring at the bottom in this area characterized by low hydrodynamic regimes. Our observation confirmed the importance of regeneration process at bottom as sources of nutrients in NA [Degobbi and Gilmartin, 1990].

[62] The bora events increased circulation, with a strong intensification of the southeastward WACC and the waters enriched in dissolved nutrients, play an important role for phytoplankton growth along all the western coast [Penna *et al.*, 2004]. This agrees with the recent results of Marini *et al.* [2008] which observed similar process during a bora event in the winter season with possibly relevant consequences on the dissolved inorganic nutrient export from the NA.

[63] Combining nutrients measurements with currents (from ROMS) normal to the transect, dissolved inorganic nutrients transport crossing the Cesenatico-Pula transect was computed on 27 September (during the bora events) and on 5 October (after the events, during a calm phase). The southeastward and the net transports for DIN (as $\text{NH}_4 + \text{NO}_2 + \text{NO}_3$), $\text{Si}(\text{OH})_4$, PO_4 and for water, obtained from our calculation, are reported in Table 3, and compared with similar yearly estimation obtained with a different method by *Degobbi and Gilmartin* [1990].

[64] The southeastward transport (i.e., exiting from the northernmost subbasin) of nutrients on 27 September was 53% higher for DIN, 135% higher for orthosilicate and 210% higher for orthophosphate than the correspondent transports on 5 October. Interestingly, the southeastward water transport showed a more limited increase (28%), demonstrating that the increase in water flux can only partially explain the higher nutrients transport during the bora period; hence part of the increased nutrients transport must be due to processes raising the nutrients concentration, such as dissolved nutrients release by resuspension in the shallow waters of the western coastal belt.

[65] Considering the net fluxes across the transect, the modification in nutrients transport was shifting from southeastward direction (during the event) to northwestward direction (after the event). Net water transport, however, even if reduced to only 4% of the 27 September value, remained southeastward. The bora blowing before 27 September was moderate, so still higher nutrients transport values can be expected during intense events. The computed nutrient transports are in the same order of magnitude than the ones found by *Degobbi and Gilmartin* [1990]; therefore our results, albeit if relative to a limited period and a single NE wind episode, seem to indicate that bora winds are determinant for enhancing the export of nutrients from the NA. Similar conclusion on the effect of bora events enhancing the southward transport of nutrients in NA was obtained by *Grilli et al.* [2005] analyzing monthly data collected along the Cesenatico transect in the warm season. The nutrient fluxes calculated by these authors were 3–5 times lower than our values obtained during the bora: this discrepancy could in part be due to the different sampling strategies and calculations utilized, but could also evidence the high variability characterizing the nutrient horizontal fluxes and the rapid response of the system to the wind forcing.

[66] After bora, the reduced or absent net flux of nutrient out of the NA can be a combined effect of the increase in utilization of autotrophic organism inside the basin with the weak dynamic. This may also mean that, in years with limited bora events, the NA could be importing (rather than exporting) dissolved nutrients and consequently a large fraction of the land nutrients input would be metabolized in the basin, enhancing the productivity processes. More

studies are needed to confirm these hypothesis, but surely changes in the bora regimes could have (and could have had) important consequences on the biological functioning of the NA system.

[67] The sharp decrease in the surface Chl *a* and phytoplankton biomass during the bora event could be related to the mixing of surface water with higher-salinity deeper waters. At the end of the event, with weaker winds, there was a generalized increase in the chlorophyll *a*, particulate organic carbon, nitrogen and phosphorus throughout the surface layer in the NA. This trend was more marked in the western waters, southern of Po delta, and was not evident in the eastern, less productive waters south of the Istrian peninsula. South of the Po delta, the highest values of Chl *a* and DO (values > 30 $\mu\text{g L}^{-1}$ and > 160%, respectively) are related to the maximum phytoplankton activity stimulated by the nutrient input deriving both from the erosion of the thermocline and rivers inputs and by the restabilization of the water column following the input of diluted Po waters constrained along the coast by the circulation. These processes contribute to enhance the new production in the southwestern coast, considered one of the main productive areas of NA [Pugnetti et al., 2004].

[68] In the studied situation, the highest abundance of species with a high surface/volume ratio occurred and the main phytoplankton group is represented by diatoms. In the unstable conditions, such as during the bora events, the diatoms' lack of motility could be compensated by fast potential growth rates and nutrients uptake [Estrada and Berdalet, 1997].

[69] In general, the variability of environmental condition in NA affects mainly the phytoplankton abundance and biomass rather than the community composition and the most abundant taxa are common both into the coastal and offshore area, differing only for their relative importance, as already reported in several studies [Socal and Bianchi, 1989; Fonda Umani et al., 1992; Caroppo et al., 1999; Totti et al., 2000; Socal et al., 2002; Totti et al., 2002; Bernardi Aubry et al., 2004].

5. Conclusions

[70] The beginning of the study period was characterized by a typical end-of-summer stratified condition with a light low-salinity layer due to river deriving from river discharge on the surface and relatively weak currents. A series of cold bora wind events caused increased mixing and intensified the circulation, deepening the mixed layer and forming a frontal system along the western coast, typical feature of the winter period. These processes occurred within a few days, showing the rapid response of the NA to the forcing factors with relatively high energy. The cold wind events decreased SST by about 2–3°C in only a few days, mostly through vertical mixing with underlying colder water. The increased coastal current and waves due to the wind stress controlled the resuspension of the bottom sediments and their southward advection. During and after the wind events, in the western coastal areas the concentration of inorganic dissolved nutrients increase can be related to several different processes.

[71] The resuspension of bottom sediments represents an important source of nutrients for water column in this

period, that are made available in upper layer for autotrophic production in the shallower areas by means of water column mixing. Moreover the mineralization at bottom in partially mixed water column mainly occurring in the central part of basin appears an important process for nutrient budget, ultimately controlled by the strong winds. The waters, enriched in dissolved nutrients, transported southward after the bora, stimulates the phytoplankton growth in water column along the western coast, representing the triggering factor for the autumnal phytoplankton bloom in NA. The strong increase of the dissolved nutrient transport observed during the bora events suggests that these wind events could limit the eutrophication of the northernmost part of the Adriatic by exporting nutrients out of the NA and represent a key factor in the determination of nutrients budget of this epicontinental basin.

[72] **Acknowledgments.** This study has been supported by the VEC-TOR-FISR project (Italian Ministry for University and Research), by the "Anossio" project (Italian Ministry for Agriculture and Forestry), and by the ANOCSIA-FIRB project (Italian Ministry for University and Research). Special thanks to the captains and crews of R/V *Alliance* and R/V *Dallaporta*; to L. Craboledda, P. Fornasiero, and V. Zangrando for their help in the field work and laboratory analyses; and to J. Chiggiato for many helpful discussions. We are indebted to the scientists and technicians of the NURC (La Spezia, Italy) for providing CTD data and to J. Book of NRL Stennis Space Center (Mississippi, United States) for providing the ADCP data of station SS02. The paper was greatly improved by the comments from C. M. Lee and from two anonymous reviewers. The authors are particularly grateful to R. P. Signell for inviting them on the ADRIA02 cruise, for help in setting up ROMS simulations, and for valuable input in the discussion and in the preparation of this paper.

References

- Artegiani, A., D. Bregant, E. Paschini, N. Pinardi, F. Raicich, and A. Russo (1997), The Adriatic Sea general circulation. Part I: Air-sea interactions and water mass structure, *J. Phys. Oceanogr.*, **27**, 1492–1514, doi:10.1175/1520-0485(1997)027<1492:TASGCP>2.0.CO;2.
- Aspila, K. I., H. Agemian, and A. S. Y. Chau (1976), A semi-automated method for the determination of inorganic, organic and total phosphate in sediments, *Analyst (London)*, **101**, 187–197, doi:10.1039/an9760100187.
- Baric, A., G. Kuspilic, and S. Matijevic (2002), Nutrient (N, P, Si) fluxes between marine sediments and water column in coastal and open Adriatic, in *Nutrients and Eutrophication in Estuaries and Coastal Waters: Proceedings of the 31st Symposium of the Estuarine and Coastal Sciences Association*, edited by E. Orive, M. Elliott, and V. N. de Jonge, pp. 151–159, Kluwer Acad., Boston, Mass.
- Beg Paklar, G., V. Isakov, D. Koraćin, V. Kourafalou, and M. Orlić (2001), A case study of bora-driven flow and density changes on the Adriatic shelf (January 1987), *Cont. Shelf Res.*, **21**, 1751–1783, doi:10.1016/S0278-4343(01)00029-2.
- Beg Paklar, G., N. Žagar, M. Žagar, R. Vellore, D. Koraćin, P.-M. Poulain, M. Orlić, I. Vilibić, and V. Dadić (2008), Modeling the trajectories of satellite-tracked drifters in the Adriatic Sea during a summertime bora event, *J. Geophys. Res.*, **113**, C11S04, doi:10.1029/2007JC004536.
- Bergamasco, A., and M. Gačić (1996), Baroclinic response of Adriatic Sea to an episode of bora wind, *J. Phys. Oceanogr.*, **26**, 1354–1369, doi:10.1175/1520-0485(1996)026<1354:BR0TAS>2.0.CO;2.
- Bergamasco, A., T. Oguz, and P. Malanotte Rizzoli (1999), Modeling dense water mass formation and winter circulation in the northern and central Adriatic Sea, *J. Mar. Syst.*, **20**, 279–300, doi:10.1016/S0924-7963(98)00087-6.
- Bernardi Aubry, F., A. Berton, M. Bastianini, G. Socal, and F. Aciri (2004), Phytoplankton succession in a coastal area of the NW Adriatic over 10 years of samplings (1990–1999), *Cont. Shelf Res.*, **24**, 97–115, doi:10.1016/j.csr.2003.09.007.
- Bignami, F., R. Sciarra, S. Carniel, and R. Santoleri (2007), Variability of Adriatic Sea coastal turbid waters from SeaWiFS imagery, *J. Geophys. Res.*, **112**, C03S10, doi:10.1029/2006JC003518.
- Booij, N., R. C. Ris, and L. H. Holthuijsen (1999), A third-generation wave model for coastal regions: 1. Model description and validation, *J. Geophys. Res.*, **104**, 7649–7666, doi:10.1029/98JC02622.

- Book, J. W., R. P. Signell, and H. Perkins (2007), Measurements of storm and non-storm circulation in the northern Adriatic: October 2002 through April 2003, *J. Geophys. Res.*, *112*, C11S92, doi:10.1029/2006JC003556.
- Brambati, A., M. Ciabatti, G. P. Fanzutti, F. Marabini, and R. Marocco (1983), A new sedimentological textural map of northern Adriatic Sea, *Boll. Oceanol. Teor. Appl.*, *1*, 267–271.
- Carniel, S., J. C. Warner, J. Chiggiato, and M. Sclavo (2009), Investigating the impact of surface wave breaking on modeling the trajectories of drifters in the northern Adriatic Sea during a wind-storm event, *Ocean Modell.*, doi:10.1016/j.ocemod.2009.07.001, in press.
- Caroppo, C., A. Fiocca, P. Sammarco, and G. Magazzù (1999), Seasonal variations of nutrients and phytoplankton in the coastal SW Adriatic Sea (1995–1997), *Bot. Mar.*, *42*, 389–400, doi:10.1515/BOT.1999.045.
- Cattaneo, A., A. Correggiati, L. Langone, and F. Trincardi (2003), The late-Holocene Gargano subaqueous delta, Adriatic shelf: Sediment pathways and supply fluctuations, *Mar. Geol.*, *193*, 61–91, doi:10.1016/S0025-3227(02)00614-X.
- Cavaleri, L. (2002), Testing and application of a third generation model in the Mediterranean Sea, progress report, Eur. Cent. for Medium-Range Weather Forecasts, Reading, U. K. (Available at http://www.ecmwf.int/about/special_projects/cavaleri_med.seawam3/report_2002.pdf.)
- Cavaleri, L., and L. Bertotti (1997), In search of the correct wind and wave fields in a minor basin, *Mon. Weather Rev.*, *125*, 1964–1975, doi:10.1175/1520-0493(1997)125<1964:ISOTCW>2.0.CO;2.
- Chapman, D. C. (1985), Numerical treatment of cross-shelf open boundaries in a barotropic coastal ocean model, *J. Phys. Oceanogr.*, *15*, 1060–1075, doi:10.1175/1520-0485(1985)015<1060:NTOCSSO>2.0.CO;2.
- Cushman-Roisin, B., and C. E. Naimie (2002), A finite element model of the Adriatic tides, *J. Mar. Syst.*, *37*, 279–297, doi:10.1016/S0924-7963(02)00204-X.
- Degobbi, D., and M. Gilmartin (1990), Nitrogen, phosphorus, and biogenic silicon budgets for the northern Adriatic Sea, *Oceanol. Acta*, *13*, 31–45.
- Dorman, C. E., et al. (2006), February 2003 marine atmospheric conditions and the bora over the northern Adriatic, *J. Geophys. Res.*, *111*, C03S03, doi:10.1029/2005JC003134.
- Eslinger, D. L., and R. L. Iverson (2001), The effects of convective and wind-driven mixing on spring phytoplankton dynamics in the southeastern Bering Sea middle shelf domain, *Cont. Shelf Res.*, *21*, 627–650, doi:10.1016/S0278-4343(00)0106-0.
- Estrada, M., and E. Berdalet (1997), Phytoplankton in a turbulent world, *Sci. Mar.*, *61*, 125–140.
- Fain, A. M. V., A. S. Ogston, and R. W. Sternberg (2007), Sediment transport event analysis on the western Adriatic continental shelf, *Cont. Shelf Res.*, *27*, 431–451, doi:10.1016/j.csr.2005.03.007.
- Fairall, C. W., E. F. Bradley, J. E. Hare, A. A. Grachev, and J. B. Edson (2003), Bulk parameterization of air-sea fluxes: Updates and verification for the COARE algorithm, *J. Clim.*, *16*, 571–591, doi:10.1175/1520-0442(2003)016<0571:BPOASF>2.0.CO;2.
- Fanning, K. A., K. L. Carder, and P. R. Betzer (1982), Sediment resuspension by coastal waters: A potential mechanism for nutrient re-cycling on the ocean's margins, *Deep Sea Res., Part A*, *29*, 953–965, doi:10.1016/0198-0149(82)90020-6.
- Flather, R. A. (1976), A tidal model of the northwest European continental shelf, *Mem. Soc. R. Sci. Liege, Coll. 8°*, *6*, 141–164.
- Fonda Umani, S., P. Franco, E. Ghirardelli, and A. Malej (1992), Outline of oceanography and the plankton of the Adriatic Sea, in *Marine Eutrophication and Population Dynamics*, edited by G. Colombo et al., pp. 347–365, Olsen and Olsen, Fredesborg, Denmark.
- Furuya, K., and K. Harada (1995), An automated precise Winkler titration for determining dissolved oxygen on board ship, *J. Oceanogr.*, *51*, 375–383, doi:10.1007/BF02285173.
- George, D. A., P. S. Hills, and T. G. Milligan (2007), Flocculation, heavy metals (Cu, Pb, Zn) and the sand-mud transition on the Adriatic continental shelf, Italy, *Cont. Shelf Res.*, *27*, 475–488, doi:10.1016/j.csr.2005.06.013.
- Giani, M., A. Boldrin, G. Mateucci, F. Frascari, M. Gismondì, and S. Rabitti (2001), Downward fluxes of particulate carbon, nitrogen and phosphorus in the north-western Adriatic Sea, *Sci. Total Environ.*, *266*, 125–134, doi:10.1016/S0048-9697(00)00744-0.
- Gismondì, M., M. Giani, F. Savelli, A. Boldrin, and S. Rabitti (2002), Particulate organic matter in the northern and central Adriatic, *Chem. Ecol.*, *18*, 27–38, doi:10.1080/02757540212692.
- Grilli, F., M. Marini, D. Degobbi, C. R. Ferrari, P. Fornasiero, A. Russo, M. Gismondì, T. Djakovac, R. Precali, and R. Simonetti (2005), Circulation and horizontal fluxes in the northern Adriatic Sea in the period June 1999–July 2002. Part II: Nutrients transport, *Sci. Total Environ.*, *353*, 115–125, doi:10.1016/j.scitotenv.2005.09.011.
- Harris, C. K., C. R. Sherwood, R. P. Signell, A. Bever, and J. C. Warner (2008), Sediment dispersal in the northwestern Adriatic Sea, *J. Geophys. Res.*, *113*, C11S03, doi:10.1029/2006JC003868.
- Hedges, J. I., and J. H. Stern (1984), Carbon and nitrogen determination of carbonate-containing solids, *Limnol. Oceanogr.*, *19*, 984–989.
- Hodur, R. M. (1997), The Naval Research Laboratory's Coupled Ocean/Atmosphere Mesoscale Prediction System (COAMPS), *Mon. Weather Rev.*, *125*, 1414–1430, doi:10.1175/1520-0493(1997)125<1414:TNRLSC>2.0.CO;2.
- Hodur, R. M., and J. D. Doyle (1998), The coupled ocean/atmosphere mesoscale model prediction system (COAMPS), in *Coastal Ocean Prediction, Coastal Estuarine Stud.*, vol. 56, edited by C. N. K. Mooers, pp. 125–155, AGU, Washington, D. C.
- Hodur, R. M., J. Pullen, J. Cummings, X. Hong, J. D. Doyle, P. Martin, and M. A. Rennick (2001), The Coupled Ocean/Atmosphere Mesoscale Prediction System (COAMPS), *Oceanography*, *15*, 88–98.
- Holm-Hansen, O., C. J. Lorenzen, R. W. Holmes, and J. D. H. Strickland (1965), Fluorometric determination of chlorophyll, *J. Cons. Cons. Int. Explor. Mer.*, *30*, 3–15.
- Hopkins, T. S., A. Artegiani, C. Kinder, and R. Pariente (1999), A discussion of the northern Adriatic circulation and flushing as determined from the ELNA hydrography, in *The Adriatic Sea*, edited by T. S. Hopkins et al., *Ecosyst. Res. Rep. 32 (EUR 18834)*, pp. 85–106, Eur. Comm., Brussels.
- Joordens, J. C. A., A. J. Souza, and A. Visser (2001), The influence of tidal straining and wind on suspended matter and phytoplankton distribution in the Rhine outflow region, *Cont. Shelf Res.*, *21*, 301–325, doi:10.1016/S0278-4343(00)00095-9.
- Kourafalou, V. (1999), Process studies on the Po River plume, north Adriatic Sea, *J. Geophys. Res.*, *104*, 29,963–29,985, doi:10.1029/1999JC900217.
- Krajcar, V. (2003), Statistical approach to wind induced currents in the northern Adriatic, *Geofizika*, *20*, 93–104.
- Kuzmić, M. (1991), Exploring the effects of bora over the northern Adriatic: CZCS imagery and a mathematical model prediction, *Int. J. Remote Sens.*, *12*, 207–214, doi:10.1080/01431169108929646.
- Kuzmić, M., and M. Orlić (1987), Wind inducing vertical shearing: AlpeX/Metaplex data on modelling exercise, *Ann. Geophys., Ser. B*, *5*, 103–112.
- Lee, C. M., et al. (2005), Northern Adriatic response to a wintertime bora wind event, *Eos Trans. AGU*, *86*(16).
- Lewis, C. V. W., C. Chen, and C. S. Davis (2001), Effect of winter wind variability on plankton transport over Georges Bank, *Deep Sea Res., Part II*, *48*, 137–158, doi:10.1016/S0967-0645(00)00083-7.
- Lukšić, I. (1975), Bora in Senj (in Croatian), *Senjski Zbornik*, *6*, 467–494.
- Malanotte Rizzoli, P., and A. Bergamasco (1983), The dynamics of the coastal region of the northern Adriatic Sea, *J. Phys. Oceanogr.*, *13*, 1105–1130, doi:10.1175/1520-0485(1983)013<1105:TDOTCR>2.0.CO;2.
- Mann, K. H. (Ed.) (1982), *Ecology of Coastal Waters: A Systems Approach*, vol. 8, 322 pp., Blackwell Sci., London.
- Marini, M., B. H. Jones, A. Campanelli, F. Grilli, and C. M. Lee (2008), Seasonal variability and Po River plume influence on biochemical properties along western Adriatic coast, *J. Geophys. Res.*, *113*, C05S90, doi:10.1029/2007JC004370.
- Miserocchi, S., L. Langone, and T. Tesi (2007), Content and isotopic composition of organic carbon within a flood layer in the Po River prodelta (Adriatic Sea), *Cont. Shelf Res.*, *27*, 338–358, doi:10.1016/j.csr.2005.05.005.
- Nittrouer, C., S. Miserocchi, and F. Trincardi (2004), The PASTA project: Investigation of Po and Apennine sediment transport and accumulation, *Oceanography*, *17*, 46–57.
- Olesen, M., C. Lundsgaard, and A. Andrushaitis (1999), Influence of nutrients and mixing on the primary production and community respiration in the Gulf of Riga, *J. Mar. Syst.*, *23*, 127–143, doi:10.1016/S0924-7963(99)00054-8.
- Orlanski, I. (1976), A simple boundary condition for unbounded hyperbolic flow, *J. Comput. Phys.*, *21*, 251–269, doi:10.1016/0021-9991(76)90023-1.
- Orlić, M., M. Kuzmić, and I. Pasarić (1994), Response of the Adriatic Sea to the bora and sirocco forcing, *Cont. Shelf Res.*, *14*, 91–116, doi:10.1016/0278-4343(94)90007-8.
- Palinkas, C. M., and C. A. Nittrouer (2007), Modern sediment accumulation on the Po shelf, Adriatic Sea, *Cont. Shelf Res.*, *27*, 489–505, doi:10.1016/j.csr.2006.11.006.
- Penna, N., S. Cappellacci, and F. Ricci (2004), The influence of the Po River discharge on phytoplankton bloom dynamics along the coast line of Pesaro (Italy) in the Adriatic Sea, *Mar. Pollut. Bull.*, *48*, 321–326, doi:10.1016/j.marpolbul.2003.08.007.

- Pirazzoli, P. A., and A. Tomasin (1999), Recent abatement of easterly winds in the northern Adriatic, *Int. J. Climatol.*, *19*, 1205–1219, doi:10.1002/(SICI)1097-0088(199909)19:11<1205::AID-JOC405>3.0.CO;2-D.
- Poulain, P., and F. Raicich (2001), Forcings, in *Physical Oceanography of the Adriatic Sea*, edited by B. Cushman-Roisin et al., chap. 2, pp. 45–65, Kluwer Acad., Dordrecht, Netherlands.
- Pugnetti, A., F. Acri, L. Alberighi, D. Barletta, M. Bastianini, F. Bernardi Aubry, A. Berton, F. Bianchi, G. Socal, and C. Totti (2004), Phytoplankton photosynthetic activity and growth rates in the NW Adriatic Sea, *Chem. Ecol.*, *20*, 399–409, doi:10.1080/02757540412331294902.
- Pullen, J., J. Doyle, R. Hodur, A. Ogston, J. Book, H. Perkins, and R. P. Signell (2003), Coupled ocean-atmosphere nested modeling of the Adriatic Sea during winter and spring 2001, *J. Geophys. Res.*, *108*(C10), 3320, doi:10.1029/2003JC001780.
- Pullen, J., J. D. Doyle, T. Haack, C. Dorman, R. P. Signell, and C. M. Lee (2007), Bora event variability and the role of air-sea feedback, *J. Geophys. Res.*, *112*, C03S18, doi:10.1029/2006JC003726.
- Raicich, F. (1994), Note on the flow rates of the Adriatic rivers, *Tech. Rep. RF 02/94*, Ist. Sper. Talassograf., Cons. Naz. delle Ric., Trieste, Italy.
- Raicich, F. (1996), On the freshwater balance of the Adriatic Sea, *J. Mar. Syst.*, *9*, 305–319, doi:10.1016/S0924-7963(96)00042-5.
- Ris, R. C., L. H. Holthuijsen, and N. Booij (1999), A third-generation wave model for coastal regions 2. Verification, *J. Geophys. Res.*, *104*, 7667–7681, doi:10.1029/1998JC900123.
- Schlitzer, R. (2002), Interactive analysis and visualization of geosciences data with Ocean Data View, *Comput. Geosci.*, *28*, 1211–1218, doi:10.1016/S0098-3004(02)00040-7.
- Shchepetkin, A. F., and J. C. McWilliams (2005), The regional oceanic modeling system (ROMS): A split-explicit, free-surface, topography-following-coordinate oceanic model, *Ocean Modell.*, *9*, 347–404, doi:10.1016/j.ocemod.2004.08.002.
- Sherwood, C. R., et al. (2004), Sediment dynamics in the Adriatic Sea investigated with coupled models, *Oceanography*, *17*, 58–69.
- Signell, R. P., S. Carniel, L. Cavaleri, J. Chiggiato, J. D. Doyle, J. Pullen, and M. Sclavo (2005), Assessment of wind quality for oceanographic modelling in semi-enclosed basins, *J. Mar. Syst.*, *53*, 217–233, doi:10.1016/j.jmarsys.2004.03.006.
- Simon, N. S. (1988), Nitrogen cycling between sediment and the shallow water column in the transition zone of the Potomac River and estuary. I. Nitrate and ammonia fluxes, *Estuarine Coastal Shelf Sci.*, *26*, 483–497, doi:10.1016/0272-7714(88)90002-9.
- Smetacek, V. S. (1975), Die Sukzession des Phytoplankton der westlichen Kieler Butch, Ph.D. thesis, 151 pp., Univ. of Kiel, Kiel, Germany.
- Socal, G., and F. Bianchi (1989), Adriatico settentrionale in condizioni di stratificazione. 3. Distribuzione della biomassa e dei popolamenti fitoplanctonici (1983–84), *Boll. Oceanogr. Teor. Appl.*, 93–109.
- Socal, G., M. Monti, P. Mozetic, and F. Bianchi (1992), Phytoplankton seasonal trends in the coastal waters of the northern Adriatic Sea (ALPE ADRIA project March–July 1990), *Rapp. P. V. Reun. Comm. Int. Explor. Sci. Mer Mediter.*, *33*, 373.
- Socal, G., A. Pugnetti, L. Alberighi, and F. Acri (2002), Observations on phytoplankton productivity in relation to hydrography in the northern Adriatic, *Chem. Ecol.*, *18*, 61–73, doi:10.1080/02757540212686.
- Socal, G., et al. (2008), Hydrological and biogeochemical features of the northern Adriatic Sea in the period 2003–2006, *Mar. Ecol. Berlin*, *29*, 449–468, doi:10.1111/j.1439-0485.2008.00266.x.
- Solidoro, C., V. Bandelj, P. Barbieri, G. Cossarini, and S. Fonda Umani (2007), Understanding dynamic of biogeochemical properties in the northern Adriatic Sea by using self-organizing maps and k-means clustering, *J. Geophys. Res.*, *112*, C07S90, doi:10.1029/2006JC003553.
- Soulsby, R. L., and J. S. Damgaard (2005), Bedload sediment transport in coastal waters, *Coastal Eng.*, *52*, 673–689, doi:10.1016/j.coastaleng.2005.04.003.
- Steppeler, J., G. Doms, U. Schattler, H. W. Bitzer, A. Gassmann, U. Damrath, and G. Gregoric (2003), Meso-gamma scale forecasts using nonhydrostatic model LM, *Meteorol. Atmos. Phys.*, *82*, 75–96, doi:10.1007/s00703-001-0592-9.
- Strathmann, R. R. (1967), Estimating the organic carbon content of phytoplankton from cell volume or plasma volume, *Limnol. Oceanogr.*, *12*, 411–418.
- Strickland, J. D. H., and T. R. Parsons (1972), *A Practical Handbook of Seawater Analysis*, *Bull. Fish. Res. Board Can.*, *167*, 311 pp.
- Tengberg, A., E. Almroth, and P. Hall (2003), Resuspension and its effects on organic carbon recycling and nutrient exchange in coastal sediments: In situ measurements using new experimental technology, *J. Exp. Mar. Biol. Ecol.*, *285–286*, 119–142, doi:10.1016/S0022-0981(02)00523-3.
- Tomas, C. R. (1997), *Identifying Marine Phytoplankton*, 858 pp., Academic, San Diego, Calif.
- Totti, C., G. Civitarese, F. Acri, D. Barletta, G. Candelabri, E. Paschini, and A. Solazzi (2000), Seasonal variability of phytoplankton populations in the middle Adriatic sub-basin, *J. Plankton Res.*, *22*, 1735–1756, doi:10.1093/plankt/22.9.1735.
- Totti, C., E. M. Cucchiari, and T. Romagnoli (2002), Intra and interannual variability of phytoplankton in coastal area of Senigallia (northern Adriatic Sea) from 1988 to 2000, *Biol. Mar. Mediter.*, *9*, 391–399.
- Totti, C., M. Cangini, C. Ferrari, R. Kraus, D. Miokovic, M. Pompei, A. Pugnetti, T. Romagnoli, S. Vanucci, and G. Socal (2005), Phytoplankton-size distribution and community structure in relation to mucilage occurrence in northern Adriatic Sea, *Sci. Total Environ.*, *353*, 204–217, doi:10.1016/j.scitotenv.2005.09.028.
- Umlauf, L., and H. Burchard (2003), A generic length-scale equation for geophysical turbulence, *J. Mar. Res.*, *61*, 235–265, doi:10.1357/002224003322005087.
- Utermöhl, H. (1958), Zur Vervollkommnung der quantitativen Phytoplankton-Methodik, *Mitt. Int. Ver. Theor. Angew. Limnol.*, *9*, 1–38.
- Warner, J. C., C. R. Sherwood, H. G. Arango, and R. P. Signell (2005), Performance of four turbulence closure models implemented using a generic length scale method, *Ocean Modell.*, *8*, 81–113, doi:10.1016/j.ocemod.2003.12.003.
- Warner, J. C., C. R. Sherwood, R. P. Signell, C. K. Harris, and H. G. Arango (2008), Development of a three-dimensional, regional, coupled wave, current, and sediment-transport model, *Comput. Geosci.*, *34*, 1284–1306, doi:10.1016/j.cageo.2008.02.012.
- Yin, K., P. J. Harrison, S. Ponda, and R. J. Beamish (1995), Entrainment of nitrate in the Fraser River Estuary and its biological implications. III. Effects of winds, *Estuarine Coastal Shelf Sci.*, *40*, 545–558, doi:10.1006/ecss.1995.0037.
- Zavatarelli, M., N. Pinardi, V. H. Kourafalou, and A. Maggiore (2002), Diagnostic and prognostic model studies of the Adriatic Sea general circulation: Seasonal variability, *J. Geophys. Res.*, *107*(C1), 3004, doi:10.1029/2000JC000210.
- Zingone, A., G. Honsell, D. Marino, M. Montresor, and G. Socal (1990), Fitoplancton, in *Metodi Nell'Ecologia del Plancton Marino, Nova Thalassia*, vol. 11, edited by M. Innamorati et al., pp. 183–198, Ed. Lint, Trieste, Italy.
- Zore-Armanda, M., and M. Gačić (1987), Effects of bura on the circulation in the north Adriatic, *Ann. Geophys., Ser B*, *5*, 93–102.

F. Bernardi Aubry, A. Boldrin, and S. Carniel, Istituto di Scienze Marine, CNR, Castello 1364, I-30122 Venice, Italy. (alfredo.boldrin@ismar.cnr.it)

A. Campanelli, F. Grilli, and M. Marini, Istituto di Scienze Marine, CNR, Largo Fiera della Pesca, 2, I-60125 Ancona, Italy.

M. Giani, Department of Biological Oceanography, Istituto Nazionale di Oceanografia e di Geofisica Sperimentale, Via Auguste Piccard 54, I-34151 Trieste, Italy.

A. Russo, DISMAR, Università Politecnica delle Marche, I-60131 Ancona, Italy.